

Analytical sensitivity in topology optimization for elastoplastic composites

Junji Kato¹ · Hiroya Hoshihara¹ · Shinsuke Takase¹ · Kenjiro Terada² · Takashi Kyoya¹

Received: 15 April 2014 / Revised: 9 March 2015 / Accepted: 22 March 2015 / Published online: 15 May 2015
© Springer-Verlag Berlin Heidelberg 2015

Abstract The present study proposes a topology optimization of composites considering elastoplastic deformation to maximize the energy absorption capacity of a structure under a prescribed material volume. The concept of a so-called *multiphase material optimization*, which is originally defined for a continuous damage model, is extended to elastoplastic composites with appropriate regularization for material properties in order to regularize material parameters between two constituents. In this study, we formulate the analytical sensitivity for topology optimization considering elastoplastic deformation and its path-dependency. For optimization applying a gradient-based method, the accuracy of sensitivities is critical to obtain a reliable optimization result. The proposed analytical sensitivity method

takes the derivative of the total stress which satisfies equilibrium equation instead of that of the incremental stress and does not need implicit sensitivity terms. It is verified that the proposed method can provide highly accurate sensitivity enough to obtain reliable optimization results by comparing with that evaluated from the finite difference approach.

Keywords Topology optimization · Analytical sensitivity analysis · Elastoplasticity · Composites · Plane stress condition

1 Introduction

Structural composites such as fiber-reinforced plastic, alloy and concrete have been developed in the expectation that they will perform various functions appropriate to various purposes and usages. One of the advantages of such composites from the mechanical viewpoint is that they enable us to control the mechanical behavior of composite materials by effectively combining materials with different characteristics. This makes it possible to obtain materials with intended mechanical characteristics appropriate for the environment or conditions in which the materials will be applied.

Today, structural design intended to maximize the mechanical characteristics (advantages) of materials constituting each composite, taking into sufficient consideration their material nonlinearity, has increasingly been promoted. Often seen are structures such as metallic vibration dampers using the plastic deformation performance of low-yield-point steel alloys, fiber-reinforced concrete that prevents brittle fractures, and hysteretic damping composite rubber, which are designed to have improved toughness or energy

✉ Junji Kato
jkato@civil.tohoku.ac.jp

Hiroya Hoshihara
hoshihara@mm.civil.tohoku.ac.jp

Kenjiro Terada
tei@irides.tohoku.ac.jp

Takashi Kyoya
kyoya@civil.tohoku.ac.jp

¹ Mechanics of Materials Laboratory,
Tohoku University, 6-6, Aoba, Aramaki, Aoba-ku,
SENDAI 980-8579, Japan

² International Research Institute of Disaster Science,
Tohoku University, 468-1, Aoba, Aramaki, Aoba-ku,
SENDAI 980-0845, Japan

absorption capacity based on their plasticity. Since design taking into consideration such complex mechanical behavior is extremely difficult, computer-based numerical experiments are employed to find an optimal structure that satisfies intended objectives or given conditions. Use of such numerical analysis techniques, however, is still not effective in finding an optimal structure, and so trial-and-error calculations end up being used. It is therefore necessary to develop a method of structural optimization to improve the energy absorption capacity of a structure through effective use of the material nonlinearity of composites.

Meanwhile, most studies concerning structural optimization focus on problems relating exclusively to simple structures composed of a single, linear elastic material, because studying complex structures raises high calculation costs and is associated with difficult theories. Studies on optimization considering the material nonlinearity of a single material have reported various findings under the theme of sensitivity analysis. Regarding plastic material models, Yuge and Kikuchi (1995), Schwarz and Ramm (2001), Maute et al. (1998) and Schwarz et al. (2001) address optimization focusing on continuum models while Choi and Santos (1987), and Ohsaki and Arora (1994) discuss optimization considering elastoplastic behavior in discrete structures such as a truss structure. Bugada et al. (1999) study shape optimization focusing on continuum damage models.

As to the structural optimization of composites, many studies have addressed the problems of determining the optimal angle of fiber in a fiber-reinforced composite (Hammer 1999) (Stegmann and Lund 2005) and of determining the optimal layout of constituent materials (Gibiansky and Sigmund 2000) (Sigmund and Torquato 1997), but they mostly focus on a linear elastic regime, as do the studies focusing on a single material. Moreover, to the best of the present authors' knowledge, few studies have been reported on a method of optimization which takes into consideration both composites and material nonlinearity. For example, Swan and Kosaka (1997) study topology optimization for elastoplastic materials using the classical Voigt-Reuss mixing rules, while Bogomolny and Amir (2012) consider the Drucker-Prager plastic model in studying topology optimization for steel-reinforced concrete. Studies by Kato et al. (2009), Kato and Ramm (2013) and Amir (2013) seem to be the only reported cases that address optimization by employing continuum damage models to consider the material nonlinear behavior of composites.

The present study, therefore, discusses topology optimization, taking into consideration the elastoplastic deformation behavior of composites to determine their optimal material layout, as a way to improve the energy absorption capacity of a structure through effective use of the material nonlinearity of composites, as stated earlier.

In addressing optimization, the method of sensitivity analysis used to take account of the nonlinear behavior of a structure, and its accuracy, are important. Various studies (e.g., Kleiber et al. (1997); Kleiber and Kowalczyk (1996); Ohsaki and Arora (1994); Schwarz and Ramm (2001); Maute et al. (1998); Schwarz et al. (2001); Zhang and Kiureghian (1993); Hisada (1995)) have reported findings regarding methods of deriving sensitivity relevant to plastic materials.

A challenge in dealing with plastic materials is that their stress-strain relations become undifferentiable when they reach their yield point or unloading point, making it difficult to correctly evaluate their stress sensitivity (derivative of stress with respect to design variables) at those points. Although Ohsaki and Arora (1994) study this problem in detail, they focus only on truss structures. It is therefore necessary equally to examine continuum structures. The studies/reports on sensitivity analysis above found conditions necessary to obtain high-accuracy sensitivity to be: (i) using a consistent elastoplastic tangent modulus in the Euler-backward integration scheme (Zhang and Kiureghian 1993), and (ii) using a stress-integration method based on the return mapping algorithm and ensuring that the sensitivity conforming thereto is derived in sensitivity analysis (Hisada 1995).

Against this background, the present study, based on the method of deriving stress sensitivity proposed by Hisada (1995), aims to formulate a new method of sensitivity derivation to maximize the energy absorption capacity of composites, which is set as the objective function, and to verify the accuracy of the sensitivity obtained.

The novelty of this study is that the proposed sensitivity approach for topology optimization can provide accurate sensitivity "even without calculating the implicit derivatives with respect to design variables". Thus, we conduct neither the analytical direct differentiation method nor analytical adjoint method. Incidentally, Hisada's sensitivity approach premises the calculation of implicit derivatives with respect to design variables. This is the difference from our approach.

Furthermore, we derive the proposed sensitivity method in detail assuming not only the general three dimensional problem but also a plane stress problem which is more cumbersome to handle. This contribution may help readers' understanding and be useful in practice.

The elastoplastic material model used in the present study is the von Mises elastoplastic material model employing the linear isotropic hardening law, and for its stress integration, a backward-Euler integration scheme based on the return mapping algorithm is employed in which a consistent tangent modulus is used. Details of these are not given here as they have been provided in many documents,

though some equations necessary to explain the sensitivity derivation method are presented in the Appendix at the end of this paper.

2 Definitions of design variables and regularization

2.1 Definitions of design variables

This section defines the design variables in topology optimization for composites. The proposed topology optimization is based on the concept of the Solid Isotropic Micro-structure with Penalization of intermediate densities, or SIMP approach (Zhou and Rozvany 1991), extended to apply to composites. This concept, illustrated in Fig. 1, is intended to represent the optimal layout of a two-phase composite consisting of two solid phases. The SIMP approach, which assumes a porous body consisting of a single material, defines design variables as material densities set for each finite element. The present study, on the other hand, assuming a two-phase composite, replaces design variables with the volume fraction of the constituents. Therefore, for the j th of the elements discretized into N (number) finite elements, the design variable s_j ($j = 1, 2, \dots, N$) can be defined as follows:

$$s_j = \frac{r_j}{r_0}, \quad 0 \leq s_j \leq 1. \tag{1}$$

Here, r_j represents the volume of phase-2 at the j th element and r_0 represents the volume of the element. This means that the elements are occupied by phase-1 when $s_j = 0$ and by phase 2 when $s_j = 1$. In the case of $0 < s < 1$, elements of the two phases are mixed. Using these design variables, incidentally, optimization of a single material (porous material) can also be performed by replacing the material constant of phase-2 with that of solid material and setting 0 for the material constant of phase-1.

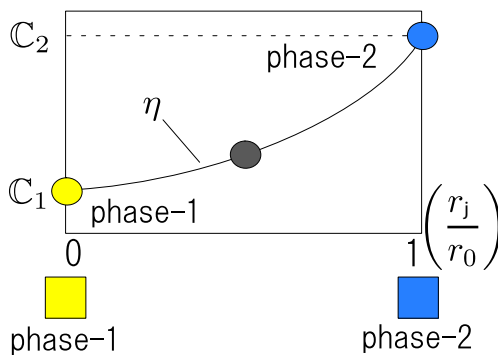


Fig. 1 Concept of two-phase material optimization

2.2 Regularization of elastoplastic material models

In this study, composite material is simply modeled by the extended SIMP like approach. Here, the material parameters in the elastoplastic model are regularized with an interpolation scheme. Appendix A provides three material parameters of the elastoplastic model; elastic stiffness tensor \mathbb{C} , work hardening modulus E^h and initial yield stress σ_y . The present study sets these effective material parameters using the design variable s_j as follows.

$$\mathbb{C}_j = \begin{cases} (1 - s_j^\eta) \mathbb{C}_1 + s_j^\eta \mathbb{C}_2 & \mathbb{C}_1 \leq \mathbb{C}_2 \\ (1 - s_j)^\eta \mathbb{C}_1 + \{1 - (1 - s_j)^\eta\} \mathbb{C}_2 & \mathbb{C}_1 > \mathbb{C}_2 \end{cases} \tag{2}$$

$$E_j^h = \begin{cases} (1 - s_j^\eta) E_1^h + s_j^\eta E_2^h & E_1^h \leq E_2^h \\ (1 - s_j)^\eta E_1^h + \{1 - (1 - s_j)^\eta\} E_2^h & E_1^h > E_2^h \end{cases} \tag{3}$$

$$(\sigma_y)_j = \begin{cases} (1 - s_j^\eta) \sigma_{y1} + s_j^\eta \sigma_{y2} & \sigma_{y1} \leq \sigma_{y2} \\ (1 - s_j)^\eta \sigma_{y1} + \{1 - (1 - s_j)^\eta\} \sigma_{y2} & \sigma_{y1} > \sigma_{y2} \end{cases} \tag{4}$$

where η is an exponential parameter. As shown above, the parameters of two materials are interpolated in smooth functions. This is called regularization. These equations are obtained by applying to plastic material a regularization method for two-phase material optimization based on the damage model of the present authors and others (Kato et al. 2009). This makes the material parameters of each element dependent on design variables, meaning that the design variables that control the topology of a structure are embedded.

3 Setting the optimization problem

The present study sets the energy absorption capacity of a composite structure subject to plastic deformation as the objective function and aims to maximize it. Absorbed energy can be expressed as the total work for displacement of the control point, and the work can be measured by the area bounded by the load-displacement curve. The constraint is that the volume of the material used in the entire structure should be constant. The objective function $f(s)$ and the equality constant $h(s)$ are set as follows:

$$\begin{aligned} \text{minimize} \quad f(s) &= - \int_{\Omega} \int_0^t \sigma : \dot{\epsilon} dt d\Omega \\ &= - \int_{\Omega} \int_{\hat{\epsilon}} \sigma : d\epsilon d\Omega, \end{aligned} \tag{5}$$

$$\text{subject to} \quad h(s) = \int_{\Omega} s_j d\Omega - \hat{V} = 0, \tag{6}$$

where, σ and ϵ represent the Cauchy stress tensor and the linear strain tensor, respectively. t and (\bullet) represent time and the time derivative, respectively. $\hat{\epsilon}$ is the total strain following the control point displacement \hat{u} , \hat{V} is the volume of phase-2 in the entire structure, and s is the design variable (vector) expressed by $s = \{s_1, \dots, s_N\}$.

Note that the objective function above is multiplied by -1 to form a minimization problem because an optimization problem is generally set as a minimization problem. The present optimization problem is solved by employing the optimality criteria (Patnaik et al. 1995).

4 Derivation of sensitivity

4.1 Derivation of sensitivity of the objective function

This section proposes a method of deriving formulae to evaluate the sensitivity of the objective function. The present study, to solve this nonlinear structural problem quasi-statically, replaces (5) with the incremental one shown below, using the pseudo-time (or load step) variable n_{step} ,

$$f(s) = \sum_{n=1}^{n_{step}} f_n(s), \tag{7}$$

where, n_{step} represents the total number of load steps. f_n indicates the value of the objective function obtained between time $n - 1$ and time n , and can be expressed as follows:

$$f_n(s) = - \int_{\Omega} \sigma_n : d\epsilon_n d\Omega. \tag{8}$$

Based on the above, the gradient of the objective function with respect to a specific design variable s_j is obtained. For the sake of simplicity, $\frac{\partial}{\partial s_j}$ shall hereafter be expressed as (∇_{s_j}) . First, the gradient of (7) can be calculated as follows:

$$\nabla_{s_j} f(s) = \sum_{n=1}^{n_{step}} \nabla_{s_j} f_n(s). \tag{9}$$

For the gradient of (8), to ensure consistency with subsequent explanations, the equation below describes the objective function value f_{n+1} obtained between time n and the current time $n + 1$,

$$\begin{aligned} \nabla_{s_j} f_{n+1} &= -\nabla_{s_j} \left(\int_{\Omega} \sigma_{n+1} : d\epsilon_{n+1} d\Omega \right) \\ &= - \int_{\Omega} \{ (\nabla_{s_j} \sigma_{n+1}) : d\epsilon_{n+1} + \sigma_{n+1} : \nabla_{s_j} d\epsilon_{n+1} \} d\Omega. \end{aligned} \tag{10}$$

Note that this paper assumes that the variables at time n are already known. Since the strain increment $d\epsilon_{n+1}$ is a variable obtained through structural analysis of the current time $n + 1$, its gradient $\nabla_{s_j} d\epsilon_{n+1}$ cannot be derived explicitly. Therefore, $\nabla_{s_j} d\epsilon_{n+1}$ is called the implicit derivative term. The present study first eliminates this $\nabla_{s_j} d\epsilon_{n+1}$ under the conditions below.

The weak form of the equilibrium equation at time $n + 1$, namely, the equation of the principle of virtual work, is as follows:

$$\int_{\Omega} \sigma_{n+1} : \delta \epsilon d\Omega - \lambda_{n+1} \int_{\Gamma_t} t_0 \cdot \delta u d\Gamma_t = 0. \tag{11}$$

Here, λ_{n+1} indicates the load factor at the current time and t_0 is the reference traction force vector, which is a constant value. Body force is neglected in this study for the sake of simplicity, without loss of generality of the equation of equilibrium. Next, since virtual displacement δu and its corresponding virtual strain $\delta \epsilon$ can be arbitrarily chosen in an equation of virtual work, replacing them with $\delta \epsilon = \nabla_{s_j} d\epsilon_{n+1}$ and $\delta u = \nabla_{s_j} du_{n+1}$ in (11) can still satisfy the equilibrium,

$$\int_{\Omega} \sigma_{n+1} : \nabla_{s_j} d\epsilon_{n+1} d\Omega - \lambda_{n+1} \int_{\Gamma_t} t_0 \cdot \nabla_{s_j} du_{n+1} d\Gamma_t = 0. \tag{12}$$

The gradient here is not related to the design variable vector s but to s_j , a component of the design variable, and therefore $\nabla_{s_j} d\epsilon_{n+1}$ (or $\nabla_{s_j} du_{n+1}$) is a tensor of the same dimension as virtual strain (or virtual displacement). As a result, there is no dimensional inconsistency, mathematically, in (12).

After presenting these equations, the present study assumes a special load condition whereby load affects the displacement control nodes alone. First, since the displacement element \hat{u} or its increment $d\hat{u}$ applied to the displacement control node is determined as a load condition regardless of the design variable s , its gradient is expressed as $\nabla_{s_j} d\hat{u} = 0$. Considering also that the reference traction force vector t_0 is always constant and does not depend on the design variable s , the displacement increment vector for the entire control node du_{n+1} (of $d\hat{u}_{n+1}$) can be identified as $t_0 \cdot \nabla_{s_j} du_{n+1} = 0$. This is the integrand of the second left-hand term of (12). Thus, (12) can be simplified as follows,

$$\int_{\Omega} \sigma_{n+1} : \nabla_{s_j} d\epsilon_{n+1} d\Omega = 0. \tag{13}$$

As a result, under this load condition, the second term of (10) can be eliminated and (10) can be rewritten as follows,

$$\nabla_{s_j} f_{n+1} = - \int_{\Omega} (\nabla_{s_j} \sigma_{n+1}) : d\epsilon_{n+1} d\Omega. \tag{14}$$

With this, the sensitivity of the objective function can be obtained by identifying the gradient of stress with respect to the design variable $\nabla_{s_j} \sigma_{n+1}$. Hereafter, $\nabla_{s_j} \sigma$ shall be called stress sensitivity.

Meanwhile, Maute et al. (1998), Schwarz et al. (2001), and Schwarz and Ramm (2001) also address optimization problems setting maximization of energy absorption capacity as the objective function. To derive sensitivity, they first define the stress increment $d\sigma_{n+1}$ as:

$$d\sigma_{n+1} = \mathbb{C}^{ep*} : d\epsilon_{n+1}, \tag{15}$$

and start by directly differentiating the stress sensitivity as follows,

$$\nabla_{s_j} d\sigma_{n+1} = \nabla_{s_j} \mathbb{C}^{ep*} : d\epsilon_{n+1} + \mathbb{C}^{ep*} : \nabla_{s_j} d\epsilon_{n+1}. \tag{16}$$

Here, \mathbb{C}^{ep*} represents the consistent tangent modulus tensor. Next, they substitute (16) into (10), add (9) and rearrange as follows:

$$\begin{aligned} \nabla_{s_j} f = & - \int_{\Omega} \int_{\hat{\epsilon}} \int_{\epsilon} (d\epsilon : \nabla_{s_j} \mathbb{C}^{ep*} : d\epsilon \\ & + 2 d\epsilon : \mathbb{C}^{ep*} : \nabla_{s_j} d\epsilon) d\Omega. \end{aligned} \tag{17}$$

Moreover, as mentioned earlier, they eliminate implicit terms by setting a special load condition, so as to propose an equation to evaluate sensitivity of the objective function as shown below,

$$\nabla_{s_j} f = - \int_{\Omega} \int_{\hat{\epsilon}} \int_{\epsilon} d\epsilon : \nabla_{s_j} \mathbb{C}^{ep*} : d\epsilon d\Omega. \tag{18}$$

This equation enables us to obtain sensitivity of the objective function merely by identifying the gradient of the tangent modulus tensor $\nabla_{s_j} \mathbb{C}^{ep*}$. It should be noted, though, that (15), which is the starting point of these processes, is formulated to identify the equilibrium point in structural analysis and therefore it may not express the stress increment correctly. In short, the equation for stress sensitivity presented by Maute et al. (1998), Schwarz et al. (2001), and Schwarz and Ramm (2001) does not aim at the sensitivity of stress that satisfies equilibrium equation. This results in an accumulation of errors in stress sensitivity as plastic deformation progresses, with particularly large errors at yield points and the points at which stress changes due to unloading, etc., or, in other words, in the vicinity of undifferentiable points.

In other words and strictly speaking, the stress increment $d\sigma_{n+1}$ or the stress $\sigma_{n+1} (= \sigma_n + \mathbb{C}^{ep*} : d\epsilon_{n+1})$ obtained from (15) don't satisfy the equilibrium equation although they satisfy the tolerance of convergence of equilibrium equation. The final stress which satisfies the equilibrium equation, denoted as $\sigma_{n+1}^{(F)}$ later, is calculated after determining equilibrium point, using obtained nodal displacement through (22) based on the return mapping algorithm, see

Section 4.3. In that sense, the incremental stress $d\sigma_{n+1}$ or the consistent tangent operator \mathbb{C}^{ep*} are simply employed as a "tool" to determine/identify the equilibrium point.

Thus, to ensure the accuracy of the sensitivity evaluation (14), the present study aims to identify the sensitivity $\nabla_{s_j} \sigma_{n+1}^{(F)}$ of the stress that satisfies the equilibrium equation. To summarize, we should directly take a derivative of $\sigma_{n+1}^{(F)}$ with respect to a design variable rather than that of σ_{n+1} and replace $\nabla_{s_j} \sigma_{n+1}$ in (14) by $\nabla_{s_j} \sigma_{n+1}^{(F)}$.

In this derivation procedure, details of which are provided in Section 4.3, $\nabla_{s_j} \sigma^{(F)}$ shall be updated taking into consideration the path-dependency in each incremental step. The procedures for conditional differentiation and for obtaining stress sensitivity described below are formulated referring to the work of Hisada (1995).

4.2 Conditional differentiation

This section outlines the concept of conditional differentiation, which is employed in the following section. In conducting optimization using an elastoplastic material model and incremental analysis, stress σ , for example, can be considered as a function composed of displacement $\mathbf{u}(s)$ and design variable s . Therefore, σ_{n+1} at the current time $n + 1$ can be expressed as

$$\begin{aligned} \sigma_{n+1} = & \sigma_{n+1}(\mathbf{u}_{n+1}(s), \mathbf{u}_n(s), \mathbf{u}_{n-1}(s), \dots, \\ & \mathbf{u}_1(s), s). \end{aligned} \tag{19}$$

This equation shows that the objective function in the n th step is determined not only by \mathbf{u}_{n+1} but also by the past history. With regard to the calculus used to solve such path-dependent problems, the variation of (19) resulting from the variation δs_j of design variables is as follows:

$$\delta \sigma_{n+1} = \frac{\partial \sigma_{n+1}}{\partial \mathbf{u}_{n+1}} \delta \mathbf{u}_{n+1} + \delta^* \sigma_{n+1}, \tag{20}$$

where,

$$\begin{aligned} \delta^* \sigma_{n+1} \equiv & \frac{\partial \sigma_{n+1}}{\partial \mathbf{u}_n} \delta \mathbf{u}_n + \frac{\partial \sigma_{n+1}}{\partial \mathbf{u}_{n-1}} \delta \mathbf{u}_{n-1} \\ & + \dots + \frac{\partial \sigma_{n+1}}{\partial \mathbf{u}_1} \delta \mathbf{u}_1 + \frac{\partial \sigma_{n+1}}{\partial s_j} \delta s_j \\ \equiv & \frac{d^* \sigma_{n+1}}{ds_j} \delta s_j. \end{aligned} \tag{21}$$

$\delta^* \sigma_{n+1}$ fixes only \mathbf{u}_{n+1} and represents the variation (conditional variation) of σ_{n+1} taking into consideration the variations of all other variables, and $d^* \sigma_{n+1}/ds_j$ similarly represents conditional variation. For the sake of simplicity, d^*/ds_j shall be expressed as $\nabla_{s_j}^*$ hereafter.

4.3 Derivation of stress sensitivity

This section explains the procedure used to obtain the stress sensitivity $\nabla_{s_j}^* \sigma_{n+1}$ at the current time $n + 1$, assuming an increment from time n to the current time $n + 1$, using the values known at time n . In this procedure, the stress sensitivity and the gradient of relevant values with respect to design variables are used as the known values for the subsequent incremental step, which enables updating of stress sensitivity taking into consideration the history up to then. Here, the conditional differentiation explained above is used to obtain gradients with respect to design variables, and gradients are all set at zero initially. Details of each of the variables presented in this section are provided in the Appendix for reference.

First, the final stress at the current time $n + 1$ is decomposed into the deviatoric and volumetric parts,

$$\sigma_{n+1}^{(F)} = \sigma'_{n+1}{}^{(F)} + p_{n+1}^{(F)} : \mathbf{I}. \tag{22}$$

Then partially differentiating both sides gives the following:

$$\nabla_{s_j}^* \sigma_{n+1}^{(F)} = \nabla_{s_j}^* \sigma'_{n+1}{}^{(F)} + \nabla_{s_j}^* p_{n+1}^{(F)} : \mathbf{I}, \tag{23}$$

where, p and \mathbf{I} are hydrostatic pressure and 2nd-order identity tensor, respectively. The two derivative terms on the right-hand side of (23) are derived separately as follows. First, we refer to some equations listed in the Appendix to obtain $\nabla_{s_j}^* \sigma'_{n+1}{}^{(F)}$.

From (62), the plastic multiplier is rewritten by substituting the final equivalent stress $\bar{\sigma}_{n+1}^{(F)}$,

$$\Delta\gamma = \frac{3}{2} \frac{\Delta\bar{\epsilon}^P}{\bar{\sigma}_{n+1}^{(F)}}, \tag{24}$$

and substituting this into (68) yields a relation of the trial and final stresses as follows:

$$\sigma'_{n+1}{}^{(F)} = \frac{1}{1 + 2G\Delta\gamma} \sigma'_{n+1}{}^{(T)}. \tag{25}$$

Here, partially differentiating (25) with $\nabla_{s_j}^*$ yields:

$$\nabla_{s_j}^* \sigma'_{n+1}{}^{(F)} = \frac{\nabla_{s_j}^* \sigma'_{n+1}{}^{(T)}}{1 + 2G\Delta\gamma} - \frac{2G\nabla_{s_j}^* (\Delta\gamma) + 2\Delta\gamma \nabla_{s_j} G}{(1 + 2G\Delta\gamma)^2} \sigma'_{n+1}{}^{(T)}. \tag{26}$$

This indicates that $\nabla_{s_j}^* \sigma'_{n+1}{}^{(T)}$, $\nabla_{s_j}^* (\Delta\gamma)$, and $\nabla_{s_j}^* G$ need to be obtained. $\nabla_{s_j}^* G$ can be easily identified because it is a component of the elastic modulus tensor of (2). As for $\nabla_{s_j}^* (\Delta\gamma)$, conducting partial differentiation of (24) with $\nabla_{s_j}^*$ yields

$$\nabla_{s_j}^* (\Delta\gamma) = \frac{3}{2} \left(\frac{\nabla_{s_j}^* (\Delta\bar{\epsilon}^P)}{\bar{\sigma}_{n+1}^{(F)}} - \frac{\Delta\bar{\epsilon}^P \nabla_{s_j}^* \bar{\sigma}_{n+1}^{(F)}}{(\bar{\sigma}_{n+1}^{(F)})^2} \right), \tag{27}$$

where $\nabla_{s_j}^* (\Delta\bar{\epsilon}^P)$ and $\nabla_{s_j}^* \bar{\sigma}_{n+1}^{(F)}$ are needed. Therefore, the following shows how to identify the three derivative terms including $\nabla_{s_j}^* (\Delta\bar{\epsilon}^P)$ and $\nabla_{s_j}^* \bar{\sigma}_{n+1}^{(F)}$, as well as $\nabla_{s_j}^* \sigma'_{n+1}{}^{(T)}$ mentioned above.

First, in accordance with the return mapping algorithm, we introduce basic equations concerning trial stress and final stress. Using (64), deviatoric stress can be expressed as follows:

$$\sigma'_{n+1}{}^{(T)} = \sigma'_n + 2G\Delta\epsilon'. \tag{28}$$

Using equation (59), an equation to express trial stress can be obtained as follows:

$$(\bar{\sigma}_{n+1}^{(T)})^2 = \frac{3}{2} (\sigma'_{n+1}{}^{(T)} : \sigma'_{n+1}{}^{(T)}). \tag{29}$$

Taking into account its dependence on design variable s , (71) is rewritten as follows:

$$\bar{\sigma}_{n+1}^{(F)} = k(\bar{\epsilon}_{n+1}^P, s). \tag{30}$$

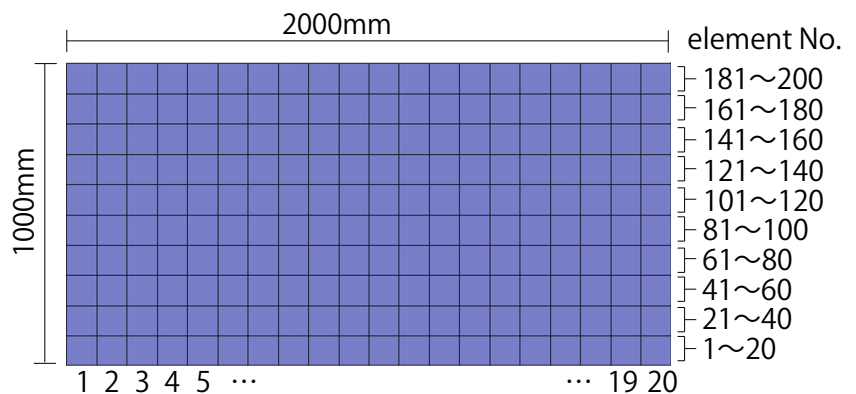
Based on (70), the relation below for trial stress and final stress can be obtained,

$$\bar{\sigma}_{n+1}^{(F)} = \bar{\sigma}_{n+1}^{(T)} - 3G\Delta\bar{\epsilon}^P. \tag{31}$$

Then partially differentiating these (28) – (31) yields the following equations, in order,

$$\nabla_{s_j}^* \sigma'_{n+1}{}^{(T)} = \nabla_{s_j}^* \sigma'_n + 2(\nabla_{s_j} G) \Delta\epsilon', \tag{32}$$

Fig. 2 Finite element mesh used for verification of sensitivity



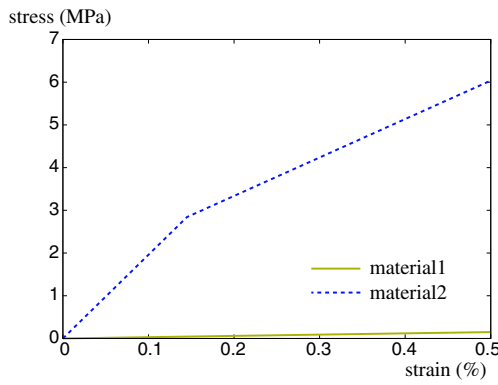


Fig. 3 Stress-strain curves based on Table 1

$$\nabla_{s_j}^* \bar{\sigma}_{n+1}^{(T)} = \frac{3}{2} \frac{1}{\bar{\sigma}_{n+1}^{(T)}} \left(\sigma'_{n+1}^{(T)} : \nabla_{s_j}^* \sigma'_{n+1}^{(T)} \right), \quad (33)$$

$$\nabla_{s_j}^* \bar{\sigma}_{n+1}^{(F)} = \frac{\partial k}{\partial \bar{\varepsilon}_{n+1}^P} \left\{ \nabla_{s_j}^* \bar{\varepsilon}_n^P + \nabla_{s_j}^* (\Delta \bar{\varepsilon}^P) \right\} + \frac{\partial k}{\partial s_j}, \quad (34)$$

$$\nabla_{s_j}^* \bar{\sigma}_{n+1}^{(F)} = \nabla_{s_j}^* \bar{\sigma}_{n+1}^{(T)} - 3 (\nabla_{s_j} G) \Delta \bar{\varepsilon}^P - 3G \nabla_{s_j}^* (\Delta \bar{\varepsilon}^P). \quad (35)$$

But the equation below is used here,

$${}^t \bar{\varepsilon}^P = {}^t \bar{\varepsilon}^P + \Delta \bar{\varepsilon}^P. \quad (36)$$

It should be noted that in deriving (32), $\nabla_{s_j}^* (\Delta \varepsilon') = 0$ is set to zero and local implicit terms are eliminated. Here, substituting (32) into (33) yields

$$\nabla_{s_j}^* \bar{\sigma}_{n+1}^{(T)} = \frac{3}{2} \frac{1}{\bar{\sigma}_{n+1}^{(T)}} \left[\sigma'_{n+1}^{(T)} : \left\{ \nabla_{s_j}^* \sigma'_{n+1} + 2 (\nabla_{s_j} G) \Delta \varepsilon' \right\} \right]. \quad (37)$$

Also substituting (34) into (35), and rearranging them with respect to $\nabla_{s_j}^* (\Delta \bar{\varepsilon}^P)$ results in the equation below,

$$\nabla_{s_j}^* (\Delta \bar{\varepsilon}^P) = \frac{\nabla_{s_j}^* \bar{\sigma}_{n+1}^{(T)} - \frac{\partial k}{\partial \bar{\varepsilon}_{n+1}^P} \nabla_{s_j}^* \bar{\varepsilon}_n^P - \frac{\partial k}{\partial s_j} - 3 (\nabla_{s_j} G) \Delta \bar{\varepsilon}^P}{\frac{\partial k}{\partial \bar{\varepsilon}_{n+1}^P} + 3G}. \quad (38)$$

This enables identification of $\nabla_{s_j}^* (\Delta \bar{\varepsilon}^P)$ using the known values. Thus, $\nabla_{s_j}^* \bar{\sigma}_{n+1}^{(F)}$ can be obtained by substituting (37) and (38) into (35).

Table 1 Material parameters for verification of sensitivities

	Material 1	Material 2
Young's modulus E	30(MPa)	1960(MPa)
Poisson's ratio ν	0.3	0.3
initial yielding stress σ_y	1.0(MPa)	2.9(MPa)
hardening modulus E^h	10(MPa)	900(MPa)

Finally, $\nabla_{s_j}^* \sigma_{n+1}^{(T)}$ can be obtained by partially differentiating (64) with $\nabla_{s_j}^*$ as follows:

$$\nabla_{s_j}^* \sigma_{n+1}^{(T)} = \nabla_{s_j}^* \sigma_n + \nabla_{s_j} C : (\varepsilon_{n+1} - \varepsilon_n). \quad (39)$$

Note that here again $\nabla_{s_j}^* (\Delta \varepsilon)$ is set to zero and local implicit terms are eliminated. Now that $\nabla_{s_j}^* (\Delta \bar{\varepsilon}^P)$, $\nabla_{s_j}^* \bar{\sigma}_{n+1}^{(F)}$, and $\nabla_{s_j}^* \sigma'_{n+1}^{(T)}$ have all been obtained, the final deviatoric stress sensitivity $\nabla_{s_j}^* \sigma'_{n+1}^{(F)}$, as shown in (26), can be identified.

Meanwhile, hydrostatic pressure is expressed as $p_{n+1}^{(F)} = \frac{1}{3} \text{tr} (\sigma_{n+1}^{(F)})$, and the relation below is derived from (66),

$$\nabla_{s_j}^* \text{tr} (\sigma_{n+1}^{(F)}) = \nabla_{s_j}^* \text{tr} (\sigma_{n+1}^{(T)}) = \text{tr} (\nabla_{s_j}^* \sigma_{n+1}^{(T)}). \quad (40)$$

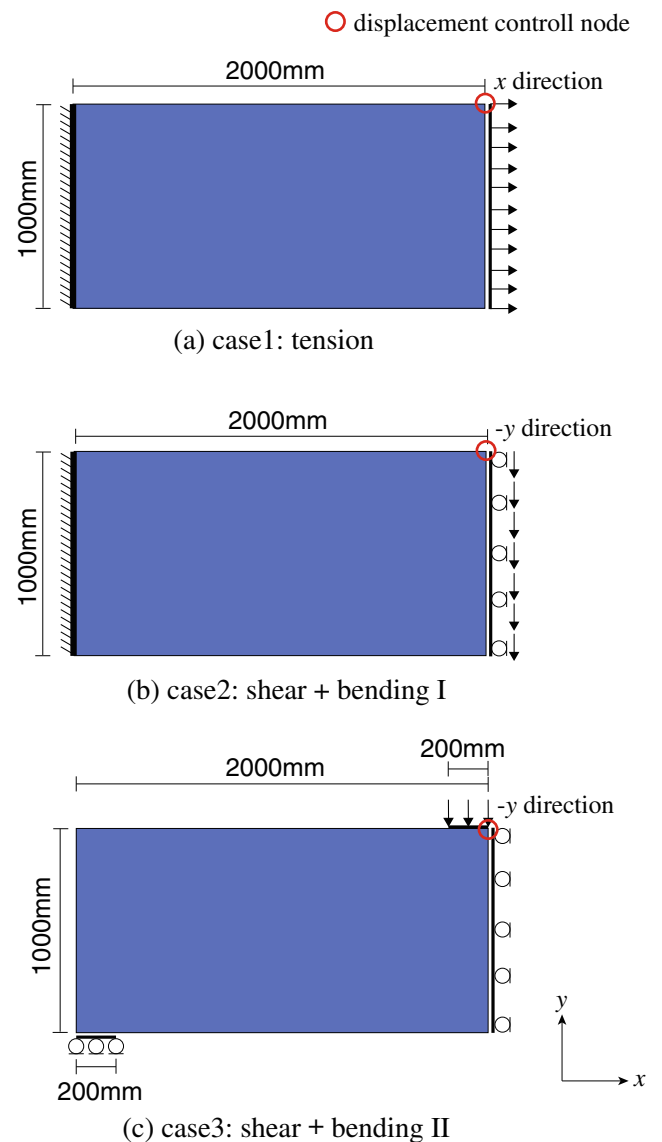


Fig. 4 Boundary conditions

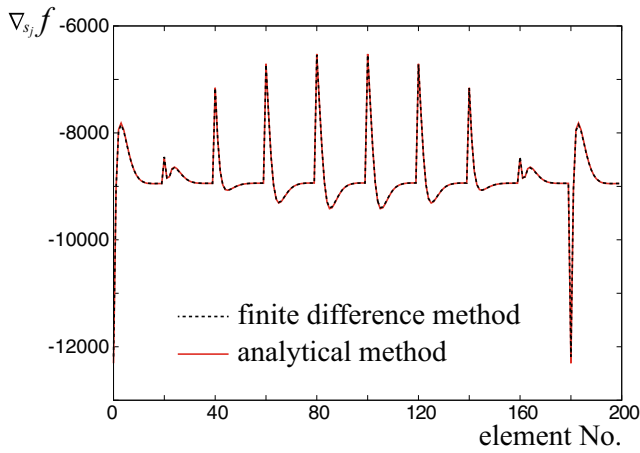


Fig. 5 Accuracy of sensitivities for case1 (tension)

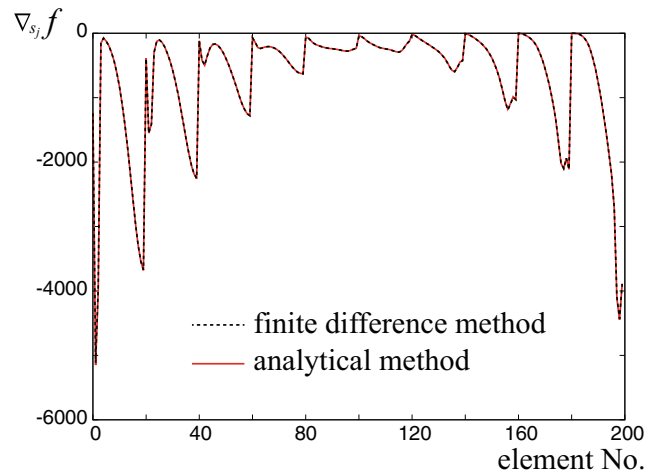


Fig. 7 Accuracy of sensitivities for case3 (shear+bending II)

Based on this, the sensitivity of hydrostatic pressure can be expressed as follows:

$$\nabla_{s_j}^* p_{n+1}^{(F)} = \frac{1}{3} \text{tr} \left(\nabla_{s_j}^* \sigma_{n+1}^{(T)} \right). \quad (41)$$

By substituting (39) into this equation, the sensitivity of hydrostatic pressure can be obtained.

Thus, the final stress sensitivity $\nabla_{s_j}^* \sigma_{n+1}^{(F)}$ can be obtained by substituting $\nabla_{s_j}^* \sigma'_{n+1}^{(F)}$ and $\nabla_{s_j}^* p_{n+1}^{(F)}$ identified here into (23). And by using this in (14), the sensitivity of the objective function which is consistent with the stress that satisfies the equilibrium equation obtained by implicit integration, can be obtained.

4.4 Stress sensitivity for plane stress condition

In the previous section, derivation of stress sensitivity assuming a return mapping algorithm for a general three

dimensional problem was presented. In this section, we formulate it assuming a plane stress problem, which is a little bit troublesome to handle but is useful in practice. The expression of a return mapping algorithm for plane stress problem is referred to Appendix B (B2), which is based on Simo and Huches (1998).

First of all, we take a derivative of (77) with respect to a design variable utilizing a conditional derivative $\nabla_{s_j}^*$ as follows:

$$\frac{1}{2} \nabla_{s_j}^* \xi - \frac{2}{3} k \cdot \left(\frac{\partial k}{\partial \bar{\varepsilon}_{n+1}^p} \nabla_{s_j}^* \bar{\varepsilon}_{n+1}^p + \frac{\partial k}{\partial s_j} \right) = 0. \quad (42)$$

Here, $\nabla_{s_j}^* \xi$ and $\nabla_{s_j}^* \bar{\varepsilon}_{n+1}^p$ can be obtained by taking a conditional derivative of (83) and (78), respectively,

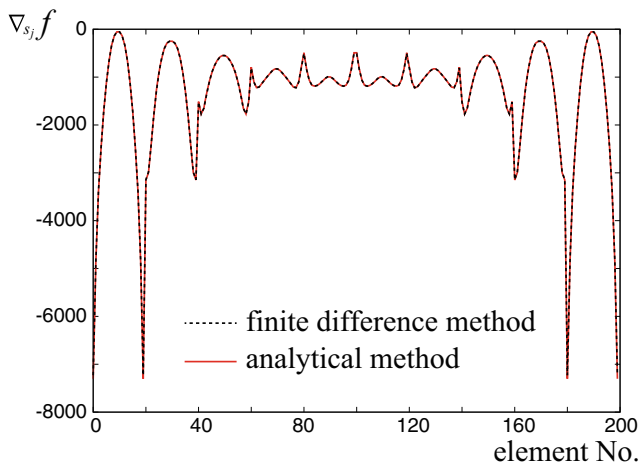


Fig. 6 Accuracy of sensitivities for case2 (shear+bending I)

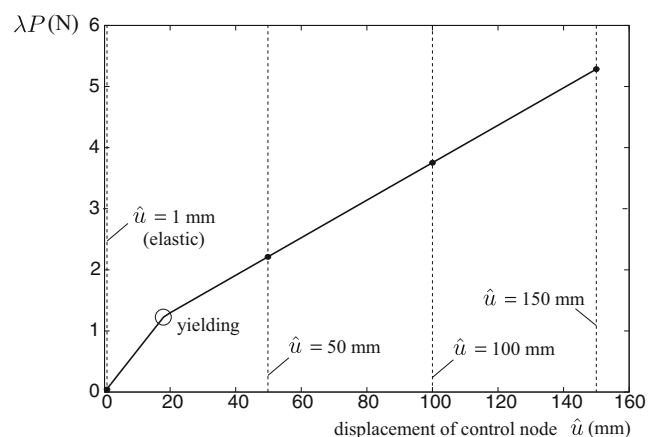


Fig. 8 Load-displacement curve of case 1 showing the degree of underlying displacements of control node

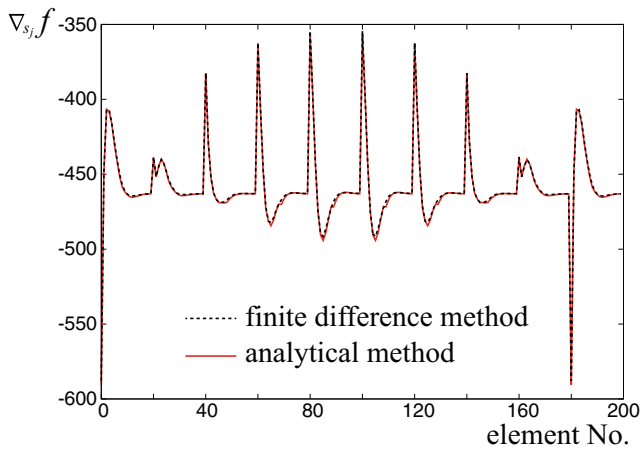


Fig. 9 Accuracy of sensitivities for case 4 (initial design variable 0.1)

$$\begin{aligned} \nabla_{s_j}^* \xi &= \frac{(\sigma_{11}^{(T)} + \sigma_{22}^{(T)}) (\nabla_{s_j}^* \sigma_{11}^{(T)} + \nabla_{s_j}^* \sigma_{22}^{(T)})}{3 [1 + E \Delta \gamma / \{3(1 - \nu)\}]^2} \\ &\quad - \frac{(\sigma_{11}^{(T)} + \sigma_{22}^{(T)})^2 \{ (\nabla_{s_j}^* E) \Delta \gamma + E \nabla_{s_j}^* (\Delta \gamma) \}}{9(1 - \nu) [1 + E \Delta \gamma / \{3(1 - \nu)\}]^3} \\ &\quad + \frac{(\sigma_{22}^{(T)} - \sigma_{11}^{(T)}) (\nabla_{s_j}^* \sigma_{22}^{(T)} - \nabla_{s_j}^* \sigma_{11}^{(T)}) + 4\sigma_{12}^{(T)} (\nabla_{s_j}^* \sigma_{12}^{(T)})}{(1 + 2G \Delta \gamma)^2} \\ &\quad - \frac{2 \{ (\sigma_{22}^{(T)} - \sigma_{11}^{(T)})^2 + 4(\sigma_{12}^{(T)})^2 \} \{ (\nabla_{s_j}^* G) \Delta \gamma + G \nabla_{s_j}^* (\Delta \gamma) \}}{(1 + 2G \Delta \gamma)^3} \end{aligned} \quad (43)$$

$$\nabla_{s_j}^* \bar{\varepsilon}_{n+1}^p = \nabla_{s_j}^* \bar{\varepsilon}_n^p + \sqrt{\frac{2}{3}} \left\{ \nabla_{s_j}^* (\Delta \gamma) \sqrt{\xi} + \frac{\Delta \gamma (\nabla_{s_j}^* \xi)}{2\sqrt{\xi}} \right\}. \quad (44)$$

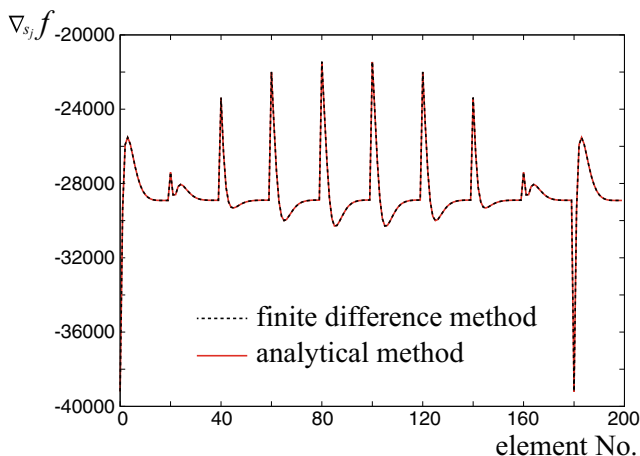


Fig. 10 Accuracy of sensitivities for case 4 (initial design variable 0.9)

Next, a derivative of the trial stress $\nabla_{s_j}^* \hat{\sigma}_{n+1}^{(T)}$ shown in Appendix B can be written by eliminating the local implicit derivative term, namely to be $\nabla_{s_j}^* (\Delta \hat{\varepsilon}) = 0$, as follows:

$$\nabla_{s_j}^* \hat{\sigma}_{n+1}^{(T)} = \nabla_{s_j}^* \hat{\sigma}_n + (\nabla_{s_j}^* C) \Delta \hat{\varepsilon}. \quad (45)$$

As can be seen, (45) consists of the explicit derivative terms only. Thus, (42) together with (43), (44) can be solved simultaneously for the unknown $\nabla_{s_j}^* (\Delta \gamma)$.

Furthermore, taking a conditional derivative of (74), (84), (85) yields,

$$\nabla_{s_j}^* \hat{\sigma}_{n+1}^{(F)} = (\nabla_{s_j}^* A) \hat{\sigma}_{n+1}^{(T)} + A (\nabla_{s_j}^* \hat{\sigma}_{n+1}^{(T)}) \quad (46)$$

where

$$\nabla_{s_j}^* A = \begin{bmatrix} \frac{1}{2} (\nabla_{s_j}^* A_{11}^* + \nabla_{s_j}^* A_{22}^*) & \frac{1}{2} (\nabla_{s_j}^* A_{11}^* - \nabla_{s_j}^* A_{22}^*) & 0 \\ \frac{1}{2} (\nabla_{s_j}^* A_{11}^* - \nabla_{s_j}^* A_{22}^*) & \frac{1}{2} (\nabla_{s_j}^* A_{11}^* + \nabla_{s_j}^* A_{22}^*) & 0 \\ 0 & 0 & \nabla_{s_j}^* A_{33}^* \end{bmatrix} \quad (47)$$

and

$$\begin{aligned} \nabla_{s_j}^* A_{11}^* &= - \frac{3(1 - \nu) \{ (\nabla_{s_j}^* E) \Delta \gamma + E \nabla_{s_j}^* (\Delta \gamma) \}}{\{3(1 - \nu) + E \Delta \gamma\}^2}, \\ \nabla_{s_j}^* A_{22}^* &= - \frac{2 \{ (\nabla_{s_j}^* G) \Delta \gamma + G \nabla_{s_j}^* (\Delta \gamma) \}}{(1 + 2G \Delta \gamma)^2}, \\ \nabla_{s_j}^* A_{33}^* &= \nabla_{s_j}^* A_{22}^*. \end{aligned} \quad (48)$$

Finally, the stress sensitivity of the final stress $\nabla_{s_j}^* \hat{\sigma}_{n+1}^{(F)}$ can be obtained by substituting $\nabla_{s_j}^* (\Delta \gamma)$ into (46)–(48).

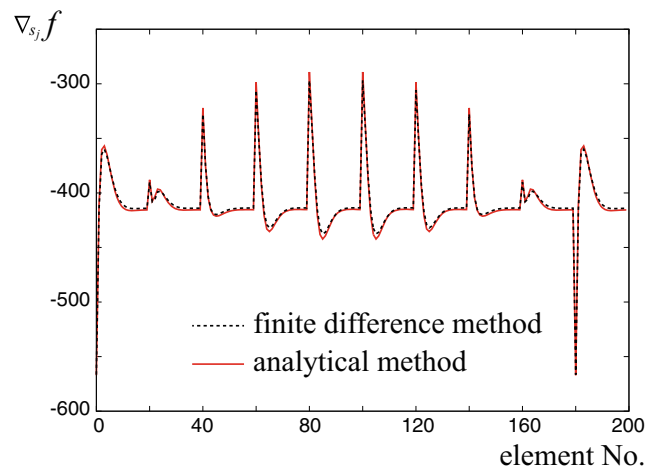


Fig. 11 Accuracy of sensitivities for case 5; $\hat{u} = 1\text{mm}$ (elastic range)

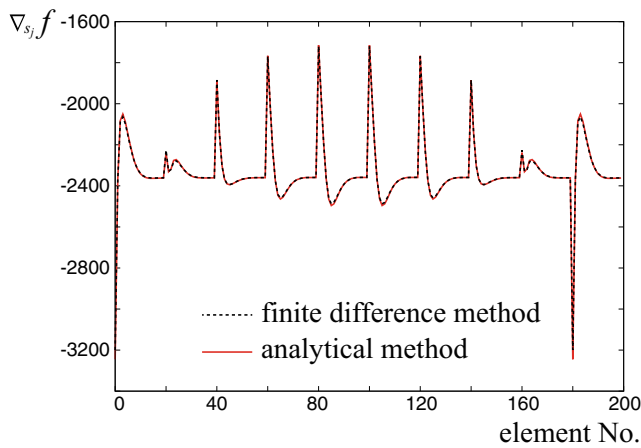


Fig. 12 Accuracy of sensitivities for case 5; $\hat{u} = 50\text{mm}$

5 Accuracy verification of derived sensitivity

5.1 Method of verification

This section presents comparative verification of the accuracy of the sensitivity of the objective function which is formulated in 4.3. The target of comparison is the sensitivity obtained by the finite difference method (FDM) as described below,

$$\nabla_{s_j} f = \frac{f(s + \Delta\tilde{s}) - f(s)}{\Delta s_j} \quad ; \quad \Delta\tilde{s}_i = \delta_{ij} \Delta s_j. \quad (49)$$

Here, δ_{ij} represents the Kronecker delta, Δs_j is a finite perturbation in design variable, and $\Delta\tilde{s}$ is a vector with all components zero except the j th component, which has Δs_j . The value of perturbation Δs_j is always 1.0×10^{-7} in this study.

Hereafter, the sensitivity obtained by the proposed method is referred to as “analytical sensitivity” to be distinguished from the “sensitivity” obtained by the FDM.

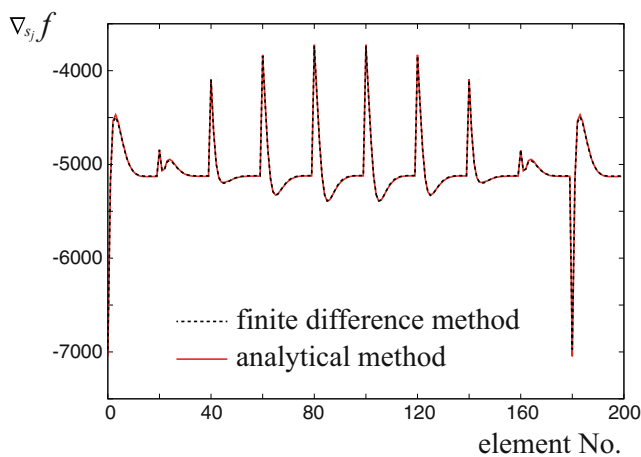


Fig. 13 Accuracy of sensitivities for case 5; $\hat{u} = 150\text{mm}$

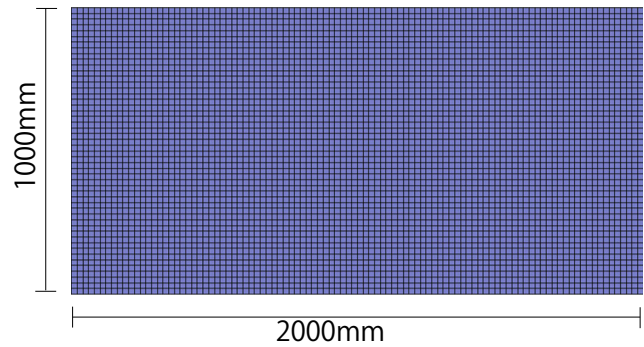


Fig. 14 Finite element mesh used for numerical calculation

5.2 Analysis models and conditions

This section describes the models used to verify the accuracy of sensitivity analysis and load conditions. As well known, sensitivity analysis using the finite difference method (FDM) requires a massive amount of calculation, and therefore we here set a small number of design variables, or, in other words, use a small number of elements. To be specific, we use a model composed of 200, eight-noded quadrilateral elements, assuming plane stress conditions. The exponential parameter $\eta = 3$ is used for each case.

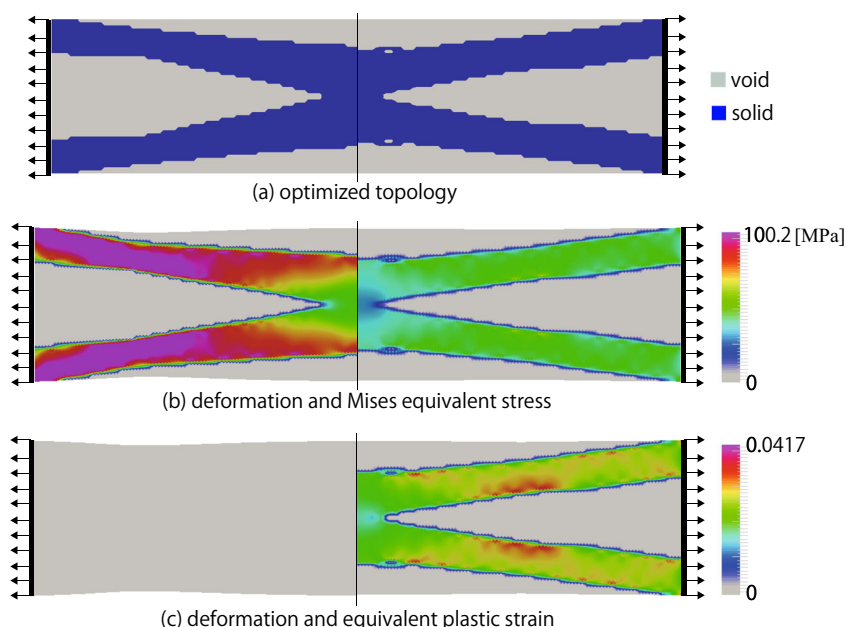
As shown in Fig. 2, each element is assigned an element number. These numbers are assigned just to make Fig. 2 clearer and are irrelevant to the actual element numbers used in the finite element analysis. As a two-phase composite is assumed, the parameters of the constituent materials are presented in Table 1 and Fig. 3. Plastic material 1 and plastic material 2 represent rubber and polypropylene, respectively. Plastic material 2 reaches its yield point with a strain of around 0.1 to 0.2%, causing plastic deformation. For these common materials and domain, we set three different constraints/load conditions below with the intention of obtaining different typical deformations.

Case 1 Tension Fig. 4(a) shows the conditions for tensile deformation. The boundary on the left side of the structure is completely fixed, and the boundary on the right side is controlled to ensure that displacement in the x -direction shows the same value at all nodes on the boundary. As to load, within the range specified in the figure, uniformly distributed load of $t_0 = 1.0\text{N/mm}$ is applied in the right-hand

Table 2 Material parameters

	Elastic	Plastic
Young’s modulus E	1960 (MPa)	1960(MPa)
Poisson’s ratio ν	0.3	0.3
initial yielding stress σ_y	∞ (MPa)	2.9(MPa)
hardening modulus E^h	∞ (MPa)	900(MPa)

Fig. 15 Optimization results for case 1 (tension): (left) elastic, (right) plastic



direction. The control point of the displacement control method is set to be the node at the upper right end. The increment of displacement is 1mm and the number of all load steps is $n = 100$ (total amount of displacement $\hat{u} = 100\text{mm}$). The initial set of design variable for each element is 0.5.

Case 2 Shear bending I Fig. 4(b) shows the conditions for shear bending deformation. The boundary on the left side of the structure is completely fixed, and the boundary on the right side is controlled to ensure that displacement in the x -direction is fixed while displacement in the y -direction shows the same value at all nodes on the boundary. As to load, within the range specified in the figure, uniformly distributed load of $t_0 = 1.0\text{N/mm}$ is applied in a downward direction. The control point of the displacement control method is the node at the upper right end. The increment of displacement is 1mm and the number of all load steps is $n = 100$ (total amount of displacement $\hat{u} = 100\text{mm}$). The initial set of design variable for each element is 0.5 again.

Case 3 Shear bending II Here, we set the conditions shown in Fig. 4(c) for another form of shear bending deformation. This analysis model represents so-called three-point bending. Uniformly distributed load of $t_0 = 1.0\text{N/mm}$ is applied in a downward direction, and the y -direction displacement of all nodes on the boundary to which load is applied is controlled similarly to the two above cases. The control point of the displacement control method is the node at the upper right end. The increment of displacement is 1mm and the number of all load steps is $n = 100$ (total amount of displacement $\hat{u} = 100\text{mm}$). The initial set of design variable for each element is the same as case 1 and 2.

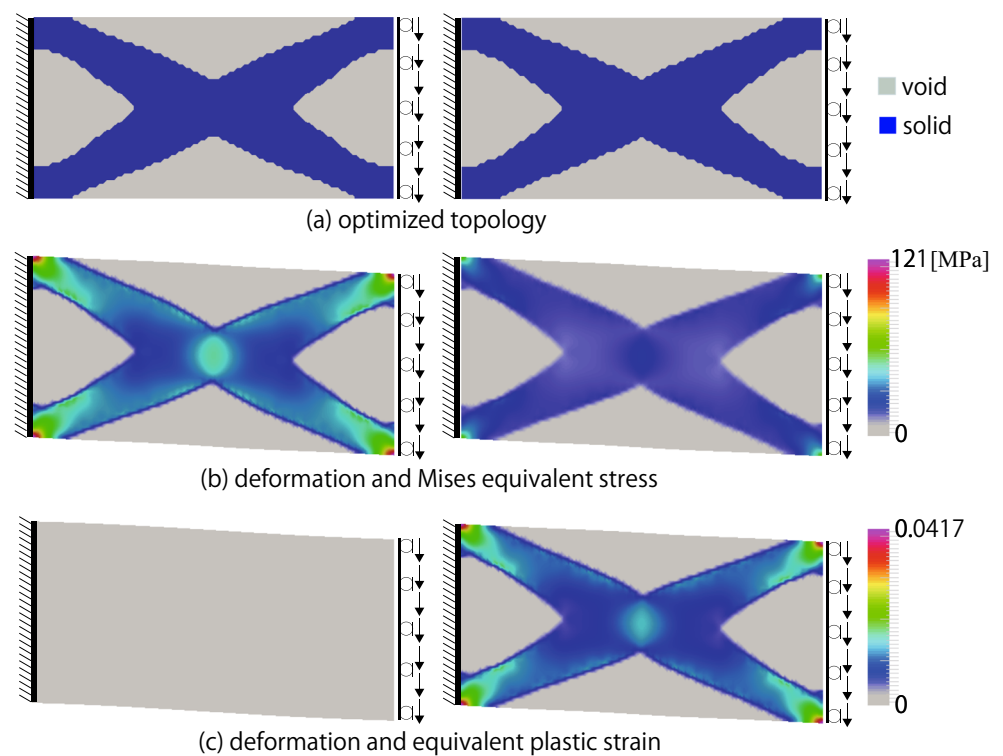
Case 4 Initial value dependency In this verification, initial value dependency using the various sets of initial design variables is focused. We employ the same condition of Case 1 and replace the initial design variable 0.5 by 0.1 and 0.9.

Case 5 Path-dependency In this verification, the influence of the degree of controlled nodal displacement \hat{u} is investigated. We employ the same condition of Case 1 and vary the total displacement controlled for $\hat{u} = 1, 50, 150\text{mm}$ in addition to $\hat{u} = 100\text{mm}$ of case 1, see Fig. 8. We assume that $\hat{u} = 1\text{mm}$ is under elastic, $\hat{u} = 50\text{mm}$ is under moderate plastic range and $\hat{u} = 150\text{mm}$ is considerably severe plastic deformation. This verification can be interpreted as the investigation of the accuracy of sensitivity for path-dependency.

5.3 Results of verification

First of all, we compare the sensitivities obtained by the finite difference method and by the analytical method under each load condition of case 1 to 3. Figs. 5, 6 and 7 show the results of the three cases of tension and shear bending I and II, respectively. All these figures have the element number plotted on the abscissa and the sensitivity of the initial optimization step on the ordinate, showing how close the sensitivity obtained at each element is to the correct value. These figures reveal that the two curves drawn for the sensitivities obtained by the finite difference method and by the analytical approach mostly overlap each other. Note that the elements presenting particularly strong sensitivity must generate remarkable plastic deformation so as to contribute to the improved absorption energy, which is the objective function.

Fig. 16 Optimization results for case 2 (shear+bending I): (left) elastic, (right) plastic



In the next, Figs. 9 and 10 display the results for case 4 employing the initial design variable 0.1 and 0.9, respectively. These results also show the high accuracy of sensitivity by the proposed analytical method.

Finally, Figs. 11, 12 and 13 introduce the results for case 5 applying $\hat{u} = 1, 50, 150\text{mm}$, respectively. As can be seen, the obtained sensitivities always have a high accuracy over the entire range from elastic to considerably severe plastic condition. If pressed to say, errors of sensitivity in Fig. 11 would seem to be slightly larger than those in others although the maximum error in Fig. 11 is at most 0.8%. This is simply because the values of sensitivity $\nabla_{s_j} f$ in Fig. 11 are relatively small compared to other cases. This relative error is not the true nature of the present verification.

Based on these results, we can conclude that sensitivity analysis by the proposed method has a high accuracy and is applicable for path-dependent problem. These results also support the validity of the structural topology obtained, in the examples of optimization calculation to be presented later.

6 Examples of optimization calculation

6.1 Analysis models and conditions

This section uses a number of optimization examples to verify the performance and validity of the structural optimization, taking into consideration the nonlinear materials

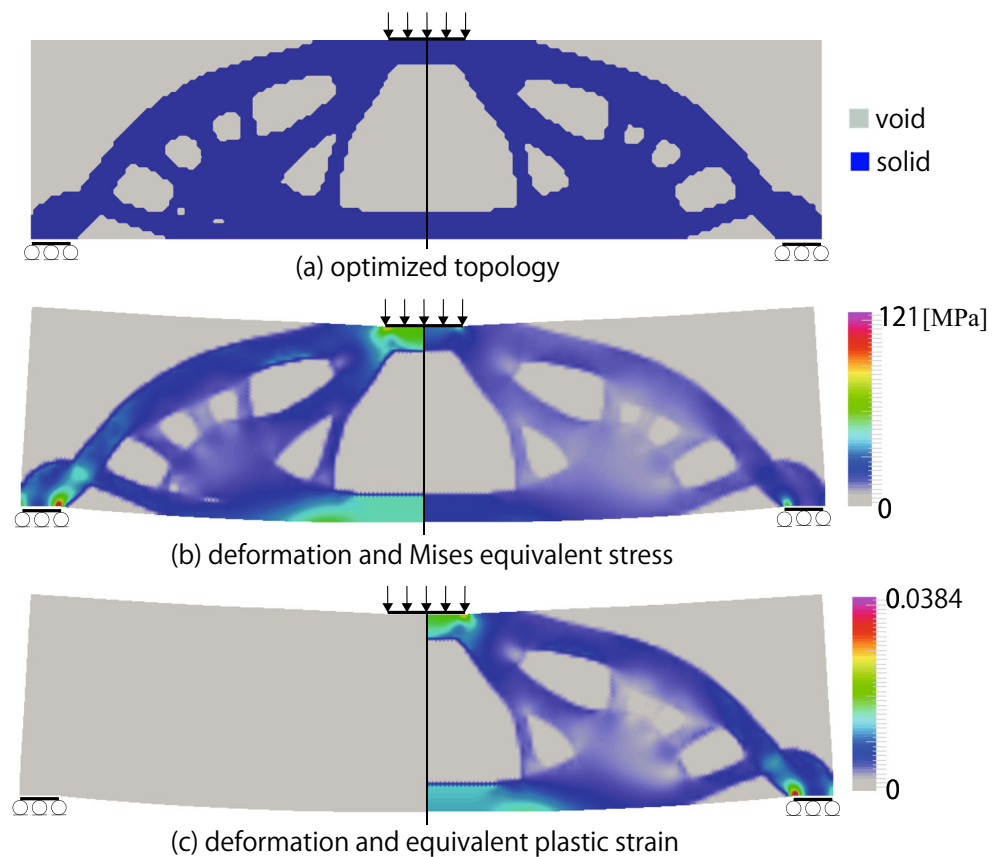
proposed in this method, and examine how the history of plastic deformation or path-dependency is reflected in the final topology. In the numerical examples below, common finite element models and load conditions are used. Fig. 14 shows the finite element mesh used for calculation. All the conditions of this model are the same as those of the model with 200 elements used in 5.2, except that the number of elements for this model is expanded to 5000 in order to obtain smooth topology. The exponential parameter $\eta = 3$ is always used for the examples.

Before verifying the topology optimization for specific composites, we conduct similar example calculations of optimization for porous materials composed of a single material and show the results. This is because it is known that a composite, even in an elastic regime, may provide an optimization topology greatly different from that of a porous material, depending on the values of the parameters of constituent materials (Bogomolny and Amir 2012), and therefore the results from optimization of composites alone may make it difficult to conceptually understand the validity of the proposed method.

6.2 Examples of optimization calculation using porous materials

Here, we observe how plastic deformation that occurs in the structure of a porous material affects the final topology. Table 2 shows the material parameters of elastic and plastic materials, which are similar to those of plastic

Fig. 17 Optimization results for case 3 (shear+bending II): (left) elastic, (right) plastic



material 2 presented in 5.2. For the elastic material, we set a sufficiently large value for yield stress so as to prevent the material yielding. Incidentally, when an elastic material is used, maximization of energy absorption capacity means the same as maximization of stiffness. Figs. 15, 16 and 17 show the results for the three conditions (tension, shear bending I and II), respectively. As reference, Fig. 18 shows the changes in the values of objective function when the plastic material of case 1 is used. Because similar results are reported regarding the changes in the objective

function values in other cases, they are omitted here to save space.

In these results, the distribution figure of each equivalent plastic strain, namely Figs. 15 to 17(c), shows a large plastic strain appearing in the plastic material, along the elements at which solid material is placed, while the distribution figure of equivalent stress, namely Figs. 15 to 17(b), shows that stress increase is regulated more in plastic material than in elastic material. This indicates that despite having the same stiffness as the elastic material, plastic material alone unquestionably causes yielding and its deformation is mostly attributable to plastic deformation. Meanwhile, under all load conditions, the topologies obtained after optimization were almost the same in both cases: using elastic material, and using plastic material. This is probably because both cases (when either material is used) have a common overall tendency for the elements

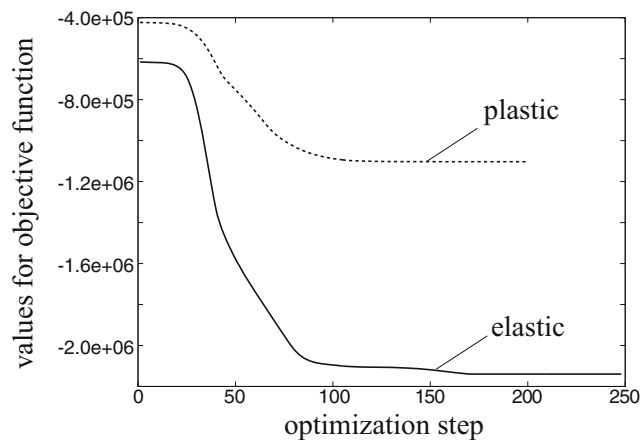


Fig. 18 Changes in value of objective function

Table 3 Material parameters

	Material 1	Material 2
Young's modulus E	210(GPa)	72(GPa)
Poisson's ratio ν	0.3	0.3
initial yielding stress σ_y	100(MPa)	505(MPa)
hardening modulus E^h	400(MPa)	1600(MPa)

subject to greater stress to have greater strain, resulting in stronger sensitivity being displayed, and thus end up with similar topologies as the optimum solution.

These results were obtained thanks largely to the mathematical approach ensuring high accuracy, which is surely a solid achievement of the present study.

6.3 Examples of optimization calculation using composites

Here, we focus on structural design in which the constituent materials of a composite have more realistic and complex nonlinearity. Table 3 shows parameters of the materials used, which are designed to have their stress-strain curves cross each other as shown in Fig. 19. Parameters were set in reference to those of low-yield-point steel (JFE-LY-100) for plastic material 1 and extra super duralumin (A7075) for plastic material 2. In dealing with these materials, it is impossible to uniformly identify which material contributes to the objective function, and the sensitivity at each element depends greatly on the amount of strain. It is therefore expected that if the degree of plastic deformation changes according to the total amount of displacement given to the displacement control point, the optimal topology will also vary greatly. This is a fundamental problem in verifying whether the proposed approach is able to evaluate path-dependency correctly.

Based on these, we set two values, $\hat{u} = 1.0\text{mm}$ and $\hat{u} = 100\text{mm}$, for the total displacement at the displacement control point, and compare the optimization results in the case in which elastic deformation is dominant and that in which plastic deformation is dominant. The total displacement of 100mm is the same value as that set for porous materials in 5.2 and the previous section. Figs. 20, 21 and

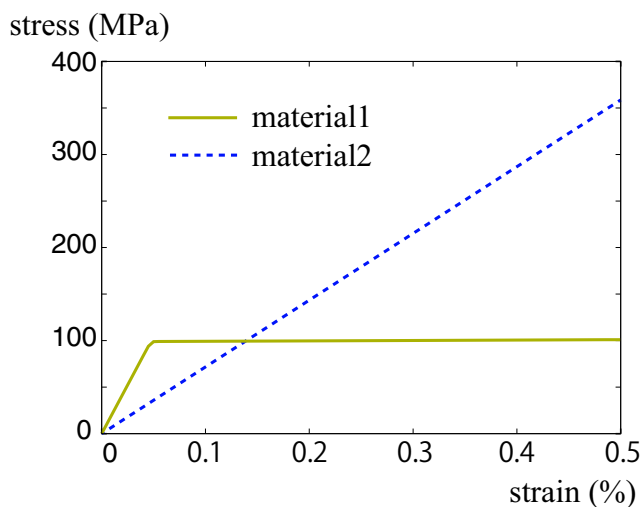


Fig. 19 Stress-strain curves

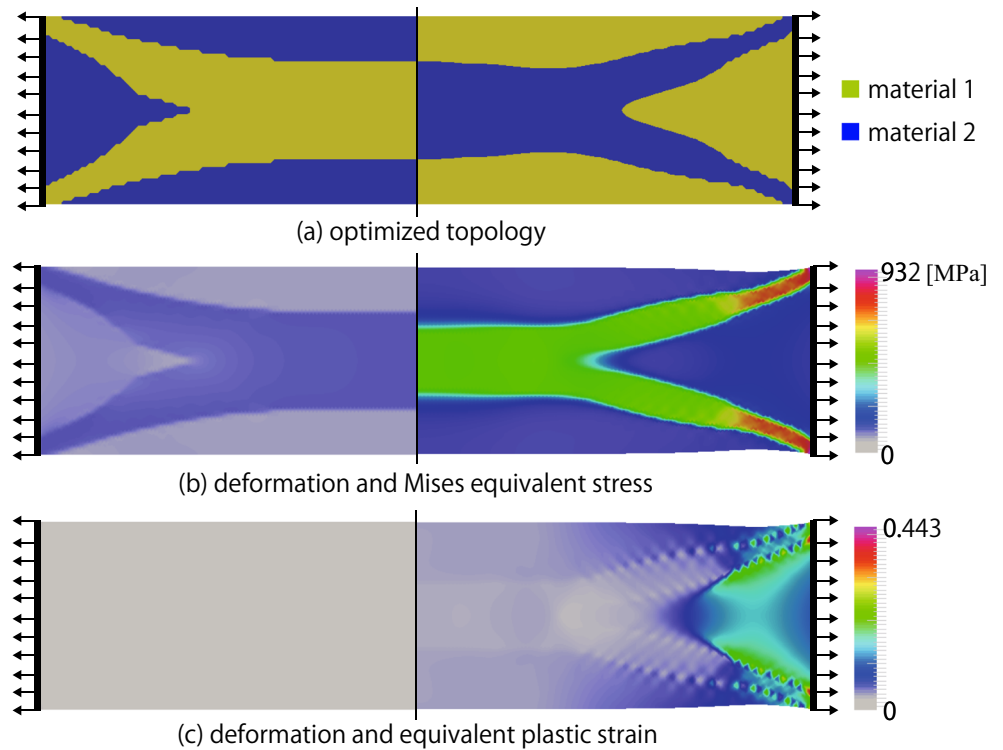
22 show the results for the three conditions (tension, shear bending I and II), respectively.

First, looking at the results under the condition of tensile deformation, we can see in Fig. 20(a) a topology in which the two materials form completely inverted shapes, though with slight variations in shape depending on the degree of displacement at the control point and the degree of plastic deformation in structure. In mechanical interpretation, this indicates that when there is little deformation in the structure, plastic material 1, which has higher initial stiffness, serves effectively as the main material in maximizing stiffness of the structure, while as deformation becomes greater, the more flexible plastic material 2 increases its importance in maximizing energy absorption capacity. We can therefore conclude that these results reflect the characteristics of composites consisting of materials with stress-strain curves that cross, and that these are the mechanically valid results of optimization. The validity of these results can also be confirmed in Fig. 20(b), which shows that the material playing the major role at each displacement carries greater stress than the other material.

Next, for shear bending I, we can see in Fig. 21(a) a tendency similar to the case of tensile deformation for the materials to form inverted shapes, but we also find the topology becoming complex at control point displacement of 100 mm. Unlike the case of tensile deformation, which causes a large amount of deformation uniformly to all elements, in the case of shear bending I the amount of strain varies among the elements, with values distributed either large or small within the design domain. This means that, for the elements that develop large plastic deformation or the elements that develop little deformation, it is easy to determine which material is effective, while for the domain involving elements that show an in-between level of strain, not very large nor very small, topology should be determined taking into consideration highly delicate structural behavior. Thus, the seemingly complex topology of Fig. 21(a) is the result of using the proposed method to quantitatively obtain a certain optimum solution to a mechanical problem that is difficult to understand intuitively. Incidentally, this calculation partially failed to achieve complete convergence of '0-1' and left some gray scale areas in the topology. This is probably because the difference in sensitivity is indistinguishable in such areas for the reason mentioned above, which was inevitable in complex problem settings. To theoretically accept such generated gray scale, employing homogenization or other technique to make the material parameters for the gray scale physically assurable may be effective. But we leave this issue for future study.

Finally, for shear bending II, we can see in Fig. 22 the same tendency as Fig. 21 for its complex topology and the gray scale remaining. Comparison of the left figure in Fig. 22(a) with that in Fig. 17(a) indicates how difficult to

Fig. 20 Optimization results for case 1 (tension) : (left) $\hat{u} = 1\text{mm}$, (right) $\hat{u} = 100\text{mm}$



understand the meaning of the obtained topology in composite even for the elastic case. This is because that although material 2 is a minor role in the elastic range, but it transfers stresses substantially over the structure unlike void; this causes in the seemingly complex topology.

Here, the authors would like to emphasize that accuracy of sensitivity is very important especially for composite material, because only the accuracy of sensitivity may be the reliable information to judge the validity of the complex optimized topology. We believe that the proposed method

Fig. 21 Optimization results for case 2 (shear+bending I): (left) $\hat{u} = 1\text{mm}$, (right) $\hat{u} = 100\text{mm}$

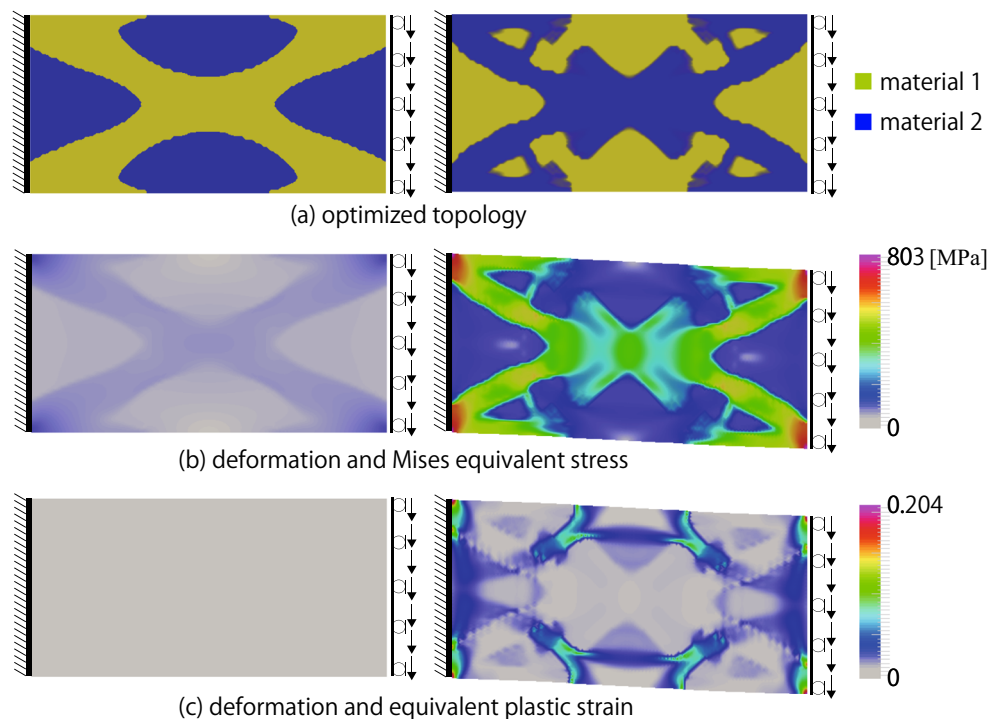
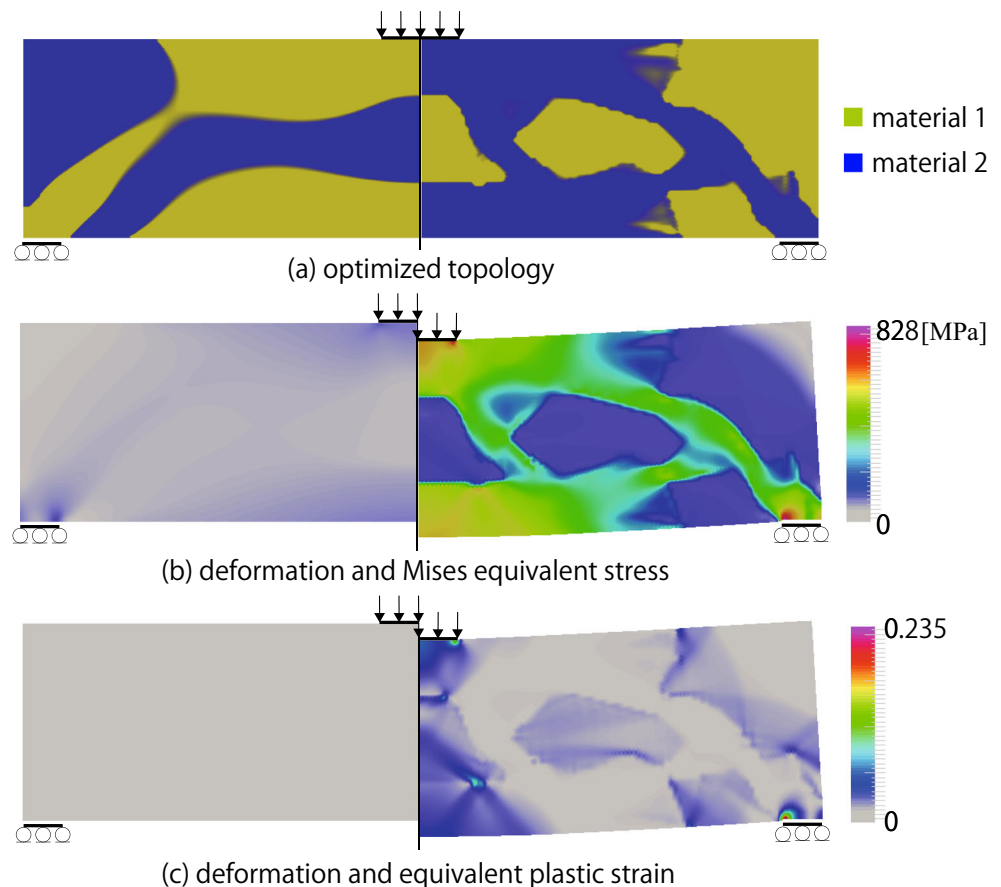


Fig. 22 Optimization results for case 3 (shear+bending II): (left) $\hat{u} = 1\text{mm}$, (right) $\hat{u} = 100\text{mm}$



can satisfy this request not only for elastic but also severe plastic deformation.

These results can be summarized as follows: Setting problems designed to generate optimization topologies that vary greatly depending on the difference in the extent of deformation, we have obtained results that are consistent with the background settings of such problems. This demonstrates that the path-dependency of plastic deformation is correctly considered in the present method.

7 Conclusion

The present study aimed to develop a topology optimization method taking into account the material nonlinearity of composites, setting maximization of the energy absorption capacity of a structure as its objective function. Targeting an isotropic elastoplastic model made by employing the von Mises yield criterion, we first regularized the parameters of each material by extending the concept of multiphase material optimization to the elastoplastic material model. We then introduced stress sensitivity consistent with the return mapping algorithm as a sensitivity analysis method, taking into consideration the elastoplastic behavior of a composite, and proposed analytical sensitivity formulae

with respect to design variables of the objective function. Finally we conducted comparative verification of the sensitivity obtained by the method proposed in the present study, and the sensitivity obtained by the finite difference method. After confirming that the proposed method assures sufficient accuracy, we conducted some example numerical calculations of optimization. The findings from these calculation examples are as follows:

- The sensitivity derived in the present study was of accuracy as high as the sensitivity obtained by the finite difference method. This illustrated the fact that stress sensitivity conforming to the stress integration according to the return mapping algorithm is crucial to secure the accuracy of sensitivity in optimization problems addressing elastoplastic materials.
- The proposed method in the present study does not need the calculation of implicit derivatives with respect to design variables. This makes coding much easier and reduces the computational costs considerably. However, the proposed method is applicable only when the external load is subject to the nodes at which the controlled DOFs of displacement are defined. This would be a fundamental reason for no implicit dependency. Although this limitation is involved, the proposed method may

be quite useful because we often meet such a structural situation in practice.

- By employing the method proposed in the present study, mechanically reasonable topologies were obtained in all the optimization calculation examples. In particular, positive results were obtained even in cases where plastic deformation was dominant in the material, proving that the proposed method is an effective optimization method capable of taking into consideration the path-dependency.
- Introducing the proposed method is expected to enable design of a composite or composite structure making effective use of the mechanical characteristics of each constituent material. Meanwhile, some optimization calculation examples showed a topology with some gray scale areas partially left. Such gray scale appeared at the elements where it is not clear which material contributes more to the improvement of the objective function, and is likely to occur in cases when the constituent materials used form stress-strain curves which cross. In fact, this gray scale phenomenon is a reasonable result, considering the settings of the relevant optimization problem.

Appendix A: Isotropic elastoplastic material model

The isotropic elastoplastic material, the return mapping algorithm and the consistent tangent modulus used in the present study are already well known and therefore detailed description of them is not necessary. However, since many of these relational equations are cited in the main text to analytically derive sensitivity in the approach formulated by the present study, we provide outlines of them in Appendix.

First, in elastoplastic deformation, the total strain tensor $\boldsymbol{\varepsilon}$ is expressed as the sum of the elastic strain tensor $\boldsymbol{\varepsilon}^e$ and the plastic strain tensor $\boldsymbol{\varepsilon}^p$ as follows:

$$\boldsymbol{\varepsilon} = \boldsymbol{\varepsilon}^e + \boldsymbol{\varepsilon}^p. \tag{50}$$

Assuming that Hooke’s law is effective during plastic deformation, the equation below can be obtained,

$$\dot{\boldsymbol{\sigma}} = \mathbb{C} : (\dot{\boldsymbol{\varepsilon}} - \dot{\boldsymbol{\varepsilon}}^p). \tag{51}$$

Here, $\boldsymbol{\sigma}$ and \mathbb{C} represent the Cauchy stress tensor and the elastic stiffness tensor, respectively, which are expressed in the velocity form herein for the sake of convenience. Assuming, by employing the von Mises yield criterion, that the yield stress changes depending only on the equivalent plastic strain $\bar{\varepsilon}^p$, the yield function Φ can be obtained as follows by using the hardening function $k(\bar{\varepsilon}^p)$,

$$\Phi(\boldsymbol{\sigma}', \bar{\varepsilon}^p) = \frac{1}{2} \boldsymbol{\sigma}' : \boldsymbol{\sigma}' - \frac{1}{3} k^2(\bar{\varepsilon}^p). \tag{52}$$

Here, $\boldsymbol{\sigma}'$ and $\bar{\varepsilon}^p$ represent the deviatoric stress tensor and the equivalent plastic strain, respectively. To make it convenient to employ the return mapping algorithm described later, the yield function is presented here in squared form. Although the hardening law for a plastic material model can be set in various ways according to the actual material, the present study assumes a simple, rate-independent, isotropic hardening law, and provides the hardening law $k(\bar{\varepsilon}^p)$ as follows:

$$k(\bar{\varepsilon}^p) = \sigma_y + E^h \bar{\varepsilon}^p, \tag{53}$$

where, σ_y and E^h represent the initial yield stress and the work-hardening modulus, respectively. Although a specific hardening law to be used for calculation is presented here, the sensitivity analysis in 4.3 describes the general hardening law in which the hardening law is represented by $k(\bar{\varepsilon}^p)$. However, kinematic hardening is not considered. From (52), the equation below is derived,

$$\frac{\partial \Phi}{\partial \boldsymbol{\sigma}} = \boldsymbol{\sigma}'. \tag{54}$$

This demonstrates that the plastic flow direction coincides with the direction of deviatoric stress $\boldsymbol{\sigma}'$. Therefore, the plastic strain rate $\dot{\boldsymbol{\varepsilon}}^p$ is obtained with $\dot{\gamma}$ as the coefficient,

$$\dot{\boldsymbol{\varepsilon}}^p = \dot{\gamma} \boldsymbol{\sigma}'. \tag{55}$$

This shows an associated flow rule in the flow theory, and $\dot{\gamma}$ shall hereafter be called the plastic multiplier. Regarding the plastic-strain work rate \dot{W}^p , the relation below is assumed,

$$\dot{W}^p = \boldsymbol{\sigma} : \dot{\boldsymbol{\varepsilon}}^p \equiv \bar{\sigma} \dot{\bar{\varepsilon}}^p, \tag{56}$$

where, $\bar{\sigma}$ and $\dot{\bar{\varepsilon}}^p$ represent the equivalent stress and the equivalent plastic strain rate, respectively. After determining the inner product of the both sides of (55) and $\boldsymbol{\sigma}$, and using the relation of (56), we can obtain the equation below,

$$\dot{\gamma} = \frac{3}{2} \frac{\dot{\bar{\varepsilon}}^p}{\bar{\sigma}}. \tag{57}$$

In the derivation of (57), the following equations are used,

$$\bar{\sigma}^2 = \frac{3}{2} (\boldsymbol{\sigma}' : \boldsymbol{\sigma}'), \tag{58}$$

$$\boldsymbol{\sigma}' : \boldsymbol{\sigma}' = \boldsymbol{\sigma} : \boldsymbol{\sigma}'. \tag{59}$$

Appendix B: Return mapping algorithm

B1: The general three dimensional expression

Incremental analysis employing an elastoplastic model assumes incremental steps from time n to $n + 1$. Subscript letters n and $n + 1$ represent the values at respective times.

(51), (55) and (57) are expressed with respect to increment as follows:

$$\boldsymbol{\sigma}_{n+1} = \boldsymbol{\sigma}_n + \mathbb{C} : (\Delta \boldsymbol{\varepsilon} - \Delta \boldsymbol{\varepsilon}^P), \quad (60)$$

$$\Delta \boldsymbol{\varepsilon}^P = \Delta \gamma \boldsymbol{\sigma}'_{n+1}, \quad (61)$$

$$\Delta \gamma = \frac{3}{2} \frac{\Delta \bar{\varepsilon}^P}{\bar{\sigma}_{n+1}}. \quad (62)$$

Substituting (61) and (62) into (60) results in the equation below,

$$\boldsymbol{\sigma}_{n+1} = \boldsymbol{\sigma}_n + \mathbb{C} : \Delta \boldsymbol{\varepsilon} - \frac{3}{2} \frac{\Delta \bar{\varepsilon}^P}{\bar{\sigma}_{n+1}} \mathbb{C} : \boldsymbol{\sigma}'_{n+1}. \quad (63)$$

Here, the known terms at time n are replaced with trial stress as follows:

$$\boldsymbol{\sigma}_{n+1}^{(T)} = \boldsymbol{\sigma}_n + \mathbb{C} : \Delta \boldsymbol{\varepsilon}. \quad (64)$$

From this, the relation of trial stress and the final stress in return mapping can be obtained,

$$\boldsymbol{\sigma}_{n+1}^{(F)} = \boldsymbol{\sigma}_{n+1}^{(T)} - \frac{3}{2} \frac{\Delta \bar{\varepsilon}^P}{\bar{\sigma}_{n+1}^{(F)}} \mathbb{C} : \boldsymbol{\sigma}'_{n+1}^{(F)}, \quad (65)$$

where, superscript letters (T) and (F) represent trial stress and the final stress, respectively. (64) obtains the trial stress at time $n + 1$ using the elastic stiffness tensor \mathbb{C} . Since the equation below is derived from (65),

$$\text{tr} \left(\boldsymbol{\sigma}_{n+1}^{(F)} \right) = \text{tr} \left(\boldsymbol{\sigma}_{n+1}^{(T)} \right) \quad (66)$$

Equation (65) can be replaced with a equation of deviatoric stress below, using the shear elastic modulus G ,

$$\boldsymbol{\sigma}'_{n+1}^{(F)} = \boldsymbol{\sigma}'_{n+1}^{(T)} - \frac{3}{2} \frac{\Delta \bar{\varepsilon}^P}{\bar{\sigma}_{n+1}^{(F)}} 2G \boldsymbol{\sigma}'_{n+1}^{(F)}. \quad (67)$$

This can be rearranged into

$$\boldsymbol{\sigma}'_{n+1}^{(F)} = \frac{\bar{\sigma}_{n+1}^{(F)}}{\bar{\sigma}_{n+1}^{(F)} + 3G \Delta \bar{\varepsilon}^P} \boldsymbol{\sigma}'_{n+1}^{(T)}, \quad (68)$$

demonstrating that the final deviatoric stress $\boldsymbol{\sigma}'_{n+1}^{(F)}$ can be expressed with a scalar multiple of the trial deviatoric stress $\boldsymbol{\sigma}'_{n+1}^{(T)}$. Moreover, because the ratio of the norm of deviatoric stress is equal to the ratio of its equivalent stress,

$$\boldsymbol{\sigma}'_{n+1}^{(F)} = \frac{\bar{\sigma}_{n+1}^{(F)}}{\bar{\sigma}_{n+1}^{(T)}} \boldsymbol{\sigma}'_{n+1}^{(T)} \quad (69)$$

can be obtained. In short, (69) obtains the final stress by correcting the trial stress in a radial direction in the deviatoric stress space. From (68) and (69), a conditional equation for the equivalent stress that makes $\boldsymbol{\sigma}'_{n+1}^{(T)}$ coincide with $\boldsymbol{\sigma}'_{n+1}^{(F)}$ is obtained,

$$\bar{\sigma}_{n+1}^{(T)} = \bar{\sigma}_{n+1}^{(F)} + 3G \Delta \bar{\varepsilon}^P. \quad (70)$$

Here, because the equivalent stress during plastic deformation coincides with the yield stress, or hardening law $k(\bar{\varepsilon}_{n+1}^P)$,

$$\bar{\sigma}_{n+1}^{(F)} = k(\bar{\varepsilon}_{n+1}^P) \quad (71)$$

can be obtained. Moreover, the equivalent plastic strain at time $n + 1$ $\bar{\varepsilon}_{n+1}^P$ can be explained as follows, using its increment $\Delta \bar{\varepsilon}^P$,

$$\bar{\varepsilon}_{n+1}^P = \bar{\varepsilon}_n^P + \Delta \bar{\varepsilon}^P. \quad (72)$$

Thus, substituting (71) and (72) into (70) and rearranging them results in

$$\Delta \bar{\varepsilon}^P = \frac{1}{3G} \left\{ \bar{\sigma}_{n+1}^{(T)} - k(\bar{\varepsilon}_n^P + \Delta \bar{\varepsilon}^P) \right\}, \quad (73)$$

where $\Delta \bar{\varepsilon}^P$ is the only unknown variable. $\Delta \bar{\varepsilon}^P$ can be obtained by solving this equation, though when a nonlinear hardening law is employed for the material model, it should be obtained by conducting repetitive calculation according to the Newton-Raphson method, etc. Then, by substituting the obtained $\Delta \bar{\varepsilon}^P$ into (70), $\bar{\sigma}_{n+1}^{(F)}$ can be obtained. Moreover, by substituting $\Delta \bar{\varepsilon}^P$ and $\bar{\sigma}_{n+1}^{(F)}$ into (62) and (68) respectively, $\Delta \gamma$ and $\boldsymbol{\sigma}'_{n+1}^{(F)}$ can be obtained.

B2: Plane stress expression

For a return mapping algorithm assuming a plane stress condition, specified constraints on stress components are considered unlike a general three dimensional problem. For this, we describe the return mapping formulation for a plane stress condition, assuming a plasticity model which has only in-plane components of stress and strain as state variables. Incidentally, the present paper refers to the expression for the plasticity model described in section 3.4 of Simo and Huchés (1998). We apply the general isotropic linear hardening law without kinematic hardening for this study and describe it in the matrix formulation.

First of all, the relation between the final stress and the trial stress can be written as follows:

$$\hat{\boldsymbol{\sigma}}_{n+1}^{(F)} = [C + \Delta \gamma P]^{-1} C \hat{\boldsymbol{\sigma}}_{n+1}^{(T)} \quad (74)$$

where $\hat{\bullet}$ means a vector of which the components are occupied by in-plane components only, such as $\hat{\boldsymbol{\sigma}} = \{\sigma_{11} \ \sigma_{22} \ \sigma_{12}\}^T$. C and P are the linear elastic constitutive matrix and the projection matrix, respectively, given by

$$C = \frac{E}{1 - \nu^2} \begin{bmatrix} 1 & \nu & 0 \\ \nu & 1 & 0 \\ 0 & 0 & \frac{1-\nu}{2} \end{bmatrix}, \quad (75)$$

$$P = \frac{1}{3} \begin{bmatrix} 2 & -1 & 0 \\ -1 & 2 & 0 \\ 0 & 0 & 6 \end{bmatrix}. \quad (76)$$

Next, the yielding condition is expressed as

$$\hat{\Phi} = \frac{1}{2} (\hat{\sigma}_{n+1}^{(F)})^T P \hat{\sigma}_{n+1}^{(F)} - \frac{1}{3} k^2 (\bar{\varepsilon}_{n+1}^P) = 0, \tag{77}$$

and the evolution law of $\bar{\varepsilon}_{n+1}^P$ can be written as follows:

$$\bar{\varepsilon}_{n+1}^P = \bar{\varepsilon}_n^P + \Delta\gamma \sqrt{\frac{2}{3} (\hat{\sigma}_{n+1}^{(F)})^T P \hat{\sigma}_{n+1}^{(F)}}. \tag{78}$$

Therefore, (74), (77), (78) can be gathered into one scalar nonlinear equation for an unknown $\Delta\gamma$ as follows:

$$\hat{\Phi} = \frac{1}{2} \xi (\Delta\gamma) - \frac{1}{3} k^2 \left(\bar{\varepsilon}_n^P + \Delta\gamma \sqrt{\frac{2}{3} \xi (\Delta\gamma)} \right) = 0, \tag{79}$$

where

$$\xi (\Delta\gamma) = (\hat{\sigma}_{n+1}^{(T)})^T A^T (\Delta\gamma) P A (\Delta\gamma) \hat{\sigma}_{n+1}^{(T)}, \tag{80}$$

and

$$A (\Delta\gamma) = [C + \Delta\gamma P]^{-1} C. \tag{81}$$

Finally, determining $\Delta\gamma$ by solving the nonlinear (79) and inserting it into (74) and (78) give the final stress sensitivity $\hat{\sigma}_{n+1}^{(F)}$ and the plastic equivalent strain $\bar{\varepsilon}_{n+1}^P$.

Furthermore, considering the mathematical characteristics of an isotropic condition, matrices P , C and A can be diagonalized by the same orthogonal matrix Q as,

$$Q = \begin{bmatrix} \frac{1}{\sqrt{2}} & \frac{1}{\sqrt{2}} & 0 \\ -\frac{1}{\sqrt{2}} & \frac{1}{\sqrt{2}} & 0 \\ 0 & 0 & 1 \end{bmatrix}. \tag{82}$$

Utilizing this diagonalization simplifies (80) and (81) as follows:

$$\xi (\Delta\gamma) = \frac{(\sigma_{11}^{(T)} + \sigma_{22}^{(T)})^2}{6 \left\{ 1 + \frac{E\Delta\gamma}{3(1-\nu)} \right\}^2} + \frac{\frac{1}{2} (\sigma_{22}^{(T)} - \sigma_{11}^{(T)})^2 + 2 (\sigma_{12}^{(T)})^2}{(1 + 2G\Delta\gamma)^2} \tag{83}$$

$$A (\Delta\gamma) = \begin{bmatrix} \frac{1}{2} (A_{11}^* + A_{22}^*) & \frac{1}{2} (A_{11}^* - A_{22}^*) & 0 \\ \frac{1}{2} (A_{11}^* - A_{22}^*) & \frac{1}{2} (A_{11}^* + A_{22}^*) & 0 \\ 0 & 0 & A_{33}^* \end{bmatrix} \tag{84}$$

$$A_{11}^* = \frac{3(1-\nu)}{3(1-\nu) + E\Delta\gamma}, \quad A_{22}^* = \frac{1}{1 + 2G\Delta\gamma}, \quad A_{33}^* = A_{22}^* \tag{85}$$

Incidentally, the expression of A is referred to de Souza Neto et al. (2000).

Appendix C: Consistent elastoplastic tangent modulus

Here, the procedure to obtain a consistent tangent modulus \mathbb{C}^{ep*} for backward-Euler integration using the variables obtained by return mapping is described.

First, substitute a 4th-order tensor \mathbb{P} that ensures $\sigma'_{n+1} = \mathbb{P} : \sigma_{n+1}$ into (60) and (61), and rearrange them to obtain

$$\begin{aligned} \sigma_{n+1} &= \sigma_n + \mathbb{C} : (\Delta\boldsymbol{\varepsilon} - \Delta\gamma \mathbb{P} : \sigma_{n+1}) \\ &= \sigma_n + \mathbb{C} : (\boldsymbol{\varepsilon}_{n+1} - \boldsymbol{\varepsilon}_n - \Delta\gamma \mathbb{P} : \sigma_{n+1}). \end{aligned} \tag{86}$$

Differentiate this equation with respect to time $n + 1$ to obtain

$$d\sigma_{n+1} = \mathbb{C} : \{d\boldsymbol{\varepsilon}_{n+1} - d(\Delta\gamma) \mathbb{P} : \sigma_{n+1} - \Delta\gamma \mathbb{P} : d\sigma_{n+1}\} \tag{87}$$

$$\iff (\mathbb{C}^{-1} + \Delta\gamma \mathbb{P}) : d\sigma_{n+1} = d\boldsymbol{\varepsilon}_{n+1} - d(\Delta\gamma) \mathbb{P} : \sigma_{n+1} \tag{88}$$

$$\iff d\sigma_{n+1} = \mathbb{C}^* : \{d\boldsymbol{\varepsilon}_{n+1} - d(\Delta\gamma) \sigma'_{n+1}\}. \tag{89}$$

Here, $\mathbb{C}^* = (\mathbb{C}^{-1} + \Delta\gamma \mathbb{P})^{-1}$ is assumed. Similarly, the equation below is obtained from (71),

$$\begin{aligned} d\bar{\sigma}_{n+1} &= \frac{\partial k}{\partial \bar{\varepsilon}^P} \Big|_{n+1} d\bar{\varepsilon}_{n+1}^P \\ &= H'_{n+1} d\bar{\varepsilon}_{n+1}^P, \end{aligned} \tag{90}$$

where, $\frac{\partial k}{\partial \bar{\varepsilon}^P} \Big|_{n+1} = H'_{n+1}$ is assumed. When the linear hardening law is employed as in the present study, $H'_{n+1} = E^h$. Moreover, because $\bar{\varepsilon}_{n+1}^P$ can be expressed as below using (62) and (72),

$$\bar{\varepsilon}_{n+1}^P = \bar{\varepsilon}_n^P + \frac{2}{3} \Delta\gamma \bar{\sigma}_{n+1}, \tag{91}$$

the derivative at time $n + 1$ is as follows:

$$d\bar{\varepsilon}_{n+1}^P = \frac{2}{3} d(\Delta\gamma \bar{\sigma}_{n+1}) + \frac{2}{3} \Delta\gamma d\bar{\sigma}_{n+1}. \tag{92}$$

Substitute this into (90) to obtain

$$\left(1 - \frac{2}{3} H'_{n+1} \Delta\gamma \right) d\bar{\sigma}_{n+1} = \frac{2}{3} H'_{n+1} d(\Delta\gamma) \bar{\sigma}_{n+1}, \tag{93}$$

$$d\bar{\sigma}_{n+1} = \frac{2}{3} \omega H'_{n+1} d(\Delta\gamma) \bar{\sigma}_{n+1}, \tag{94}$$

where, $\omega = \left(1 - \frac{2}{3} H'_{n+1} \Delta\gamma \right)^{-1}$ is assumed.

From (58), the relational equation of deviatoric stress and equivalent stress at time $n + 1$ can be obtained as follows:

$$\bar{\sigma}_{n+1}^2 = \frac{3}{2} (\boldsymbol{\sigma}'_{n+1} : \boldsymbol{\sigma}'_{n+1}). \tag{95}$$

Differentiate both sides with respect to time $n + 1$ and rearrange them to obtain

$$\bar{\sigma}_{n+1} d\bar{\sigma}_{n+1} = \frac{3}{4} d(\boldsymbol{\sigma}_{n+1} : \boldsymbol{\sigma}'_{n+1}) \tag{96}$$

$$= \frac{3}{2} d\boldsymbol{\sigma}_{n+1} : \boldsymbol{\sigma}'_{n+1}. \tag{97}$$

Note here that one of the σ'_{n+1} on the right-hand side is replaced with σ_{n+1} , using the relation of (59). Then, substitute (97) into (94) to obtain

$$d\sigma_{n+1} : \sigma'_{n+1} = \frac{4}{9} \omega H'_{n+1} d(\Delta\gamma) \bar{\sigma}_{n+1}^2. \quad (98)$$

And substitute (89) here to obtain

$$\begin{aligned} \frac{4}{9} \omega H'_{n+1} d(\Delta\gamma) \bar{\sigma}_{n+1}^2 &= \sigma'_{n+1} \\ &: [\mathbb{C}^* : \{d\boldsymbol{\varepsilon}_{n+1} - d(\Delta\gamma) \sigma'_{n+1}\}], \end{aligned} \quad (99)$$

and rearrange this with respect to $d(\Delta\gamma)$, to obtain

$$d(\Delta\gamma) = \frac{\sigma'_{n+1} : (\mathbb{C}^* : d\boldsymbol{\varepsilon}_{n+1})}{\sigma'_{n+1} : (\mathbb{C}^* : \sigma'_{n+1}) + \frac{4}{9} \omega H'_{n+1} \bar{\sigma}_{n+1}^2}. \quad (100)$$

Then substituting this into (89) results in

$$\begin{aligned} d\sigma_{n+1} &= \mathbb{C}^* : \left\{ d\boldsymbol{\varepsilon}_{n+1} - \frac{\sigma'_{n+1} : (\mathbb{C}^* : d\boldsymbol{\varepsilon}_{n+1})}{\sigma'_{n+1} : (\mathbb{C}^* : \sigma'_{n+1}) + \frac{4}{9} \omega H'_{n+1} \bar{\sigma}_{n+1}^2} \sigma'_{n+1} \right\} \\ &= \left\{ \mathbb{C}^* - \frac{(\mathbb{C}^* : \sigma'_{n+1}) \otimes (\mathbb{C}^* : \sigma'_{n+1})}{\sigma'_{n+1} : (\mathbb{C}^* : \sigma'_{n+1}) + \frac{4}{9} \omega H'_{n+1} \bar{\sigma}_{n+1}^2} \right\} : d\boldsymbol{\varepsilon}_{n+1} \\ &\equiv \mathbb{C}^{\text{ep}*} : d\boldsymbol{\varepsilon}_{n+1}, \end{aligned} \quad (101)$$

and the $\mathbb{C}^{\text{ep}*}$ in this equation turns out to be the consistent elastoplastic tangent modulus.

References

- Amir O (2013) A topology optimization procedure for reinforced concrete structures. *Comput Struct* 114–115:46–58
- Bugeda G, Gil L, Oñate E (1999) Structural shape sensitivity analysis for nonlinear material models with strain softening. *Struct Optim* 17:162–171
- Bogomolny M, Amir O (2012) Conceptual design of reinforced concrete structures using topology optimization with elastoplastic material modeling. *Int J Num Meth Eng* 90:1578–1597
- Choi KK, Santos JLT (1987) Design sensitivity analysis of nonlinear structural systems Part I: Theory. *Int J Num Meth Eng* 24: 2039–2055
- de Souza Neto EA, Perić D, Owen DRJ (2000) *Computational methods for plasticity: Theory and applications*, John Wiley & Sons, Inc.
- Gibiansky LV, Sigmund O (2000) Multiphase composites with extremal bulk modulus. *J Mech Phys Solids* 48:461–498
- Hammer VB (1999) Optimal laminate design subject to single membrane loads. *Struct Optim* 17:65–73
- Hisada T (1995) Recent Progress in Nonlinear FEM-Based Sensitivity Analysis, *JSME International Journal, Series A*, 38(3), pp. 301–310
- Kato J, Ramm E (2013) Multiphase layout optimization for fiber reinforced composites considering a damage model. *Eng Struct* 49:202–220
- Kato J, Lipka A, Ramm E (2009) Multiphase material optimization for fiber reinforced composites with strain softening. 63–81 39
- Kleiber M, Kowalczyk P (1996) Sensitivity analysis in plane stress elasto-plasticity and elasto-viscoplasticity. *Comp Meth Appl Mech Eng* 137:395–409
- Kleiber M, Antúnez H, Hien TD, Kowalczyk P (1997) *Parameter sensitivity in nonlinear mechanics*, John Wiley & Sons, Chichester, England, UK
- Maute K, Schwarz S, Ramm E (1998) Adaptive topology optimization of elastoplastic structures. *Struct Optim* 15:81–91
- Ohsaki M, Arora JS (1994) Design sensitivity analysis of elastoplastic structures. *Int J Num Meth Eng* 37:737–762
- Patnaik SN, Gupta JD, Berke L (1995) Merits and limitations of optimality criteria method for structural optimization. *Int. J. Num. Meth. Eng* 38:3087–3120
- Schwarz S, Ramm E (2001) Sensitivity analysis and optimization for non-linear structural response, *Engrg Comput*, 18, 3/4, 610–641
- Schwarz S, Maute K, Ramm E (2001) Topology and shape optimization for elastoplastic structural response. *Comput Appl Mech Engrg* 190:2135–2155
- Sigmund O, Torquato S (1997) Design of materials with extreme thermal expansion using a three-phase topology optimization method. *J Mech Phys Solids* 45(6):1037–1067
- Simo JC, Huges TJR (1998) *Computational Inelasticity*, Springer-Verlag New York, Inc.
- Stegmann J, Lund E (2005) Discrete material optimization of general composite shell structures. *Int J Num Meth Eng* 62: 2009–2027
- Swan CC, Kosaka I (1997) Voigt-Reuss topology optimization for structures with nonlinear material behaviors. *Int J Num Meth Eng* 40:3785–3814
- Yuge K, Kikuchi N (1995) Optimization of a frame structures subjected to a plastic deformation. *Struct Optim* 10:197–208
- Zhang Y, Kiureghian ADer (1993) Dynamic response sensitivity of inelastic structures. *Comp Meth Appl Mech Eng* 108:23–36
- Zhou M, Rozvany GIN (1991) The COC algorithm, part II : Topological, geometrical and generalized shape optimization. *Comp Meths Appl Mech Eng* 89:309–336